Type Ia Supernovae and Cosmology

M. Sullivan

Summary Type Ia Supernovae (SNe Ia) provide cosmologists with a precise calibrateable "standard candle" with which to probe the expansion history of the universe on large scales. Pioneering astronomical surveys in the late 1990s exploited these distant cosmic explosions to directly reveal the presence of a "dark energy," opposing the attractive, slowing force of gravity and instead accelerating the universe's rate of expansion. Dark energy has since emerged as being responsible for more than 70% of the universe's mass–energy: the lack of a viable theoretical explanation has sparked an intense observational effort to understand its nature. In this chapter we review the use of SNe Ia in cosmology and dark energy studies. We begin by placing the SNe Ia in a cosmological context, introducing the framework in which their physical fluxes are interpreted, and discussing their underlying physics which leads to their near-uniform peak brightness, exploited by astronomers to estimate distances. We show how advances in the empirical understanding of SNe Ia led to the direct discovery of the accelerating universe and how modern SN Ia searches and distance estimation techniques, combined with complementary probes of large-scale structure such as baryon acoustic oscillations, have measured the average equation of state of dark energy to better than 5% (statistical error). Systematics are now of increasing importance and we discuss the main sources of these, both experimental and astrophysical, together with an experimental error budget typical of that in a modern SN Ia survey. Finally, we outline the future prospects for measuring dark energy with SN Ia using the next generation of planned experiments.

1 Introduction

The newest puzzle in cosmology is the observed acceleration of the expansion of the universe. The universe has been known to be expanding, and not static and unchanging, since the beginning of the twentieth century. The early work of Slipher, Hubble,

M. Sullivan (✉)
Department of Physics (Astrophysics), DWB, Keble Road, Oxford, OX1 3RH, UK
e-mail: sullivan@astro.ox.ac.uk

Sullivan, M.: *Type Ia Supernovae and Cosmology*. Lect. Notes Phys. **800**, 59–97 (2010)
DOI 10.1007/978-3-642-10598-2_2

and Humason [1, 2] showed that nearby "spiral nebulae" are receding from the Earth in every direction on the sky with velocities proportional to their inferred distance, implying that the universe is getting larger over time, expanding in every direction. For a universe filled with matter and radiation, general relativity (GR) predicts that the gravitational attraction of the matter in the universe should lead to a *deceleration* in this expansion rate as the universe grows and ages. However, observations over the last decade have shown the exact opposite: the rate of the expansion is increasing with time; the expansion of the universe is *accelerating*. This "cosmic acceleration" has been confirmed with a wide variety of different astrophysical observations, and the data indicating this acceleration are now not seriously in question. *However, the physical reason for the observed cosmic acceleration remains a complete mystery.*

Two broad possibilities are generally considered. The first is that around 70% of the matter–energy density of the universe exists in an as yet unknown form, coined "dark energy," the key characteristic of which is a strong negative pressure which pushes the universe apart. There exists no compelling or elegant explanation for the presence or nature of this dark energy, or the magnitude of its observed influence, although various theoretical possibilities have been postulated [e.g., 3, 4]. Dark energy could be in the form of a vacuum energy, filling the universe and constant in space and time – a "Cosmological Constant." Alternatively, dark energy may be dynamical, a rolling scalar energy field which varies with both time and location ("quintessence" theories).

A second possibility is that the observed cosmic acceleration is an artifact of our incomplete knowledge of physical laws of gravity in the universe, in particular that the laws of GR, a foundation of modern physics, simply break down on the largest scales. The implication of this is that the cosmological framework in which we interpret astronomical observations is incorrect, and this is manifested in observational data as an acceleration in the expansion rate. These ideas are collectively known as "modified gravity" theories. Such theories are constrained in that they must be essentially equivalent to GR on scales of the solar system, where GR is stunningly successful, and also in the early universe where the predictions of standard cosmology match observational effects such as the properties of the cosmic microwave background and the growth of large-scale structure [5]. Nonetheless, a confirmation of this alternative explanation for the observed acceleration would be as profound as the existence of dark energy itself.

Either of these possibilities would revolutionize our understanding of the laws governing the physical evolution of the universe. Understanding the cosmic acceleration has, therefore, rapidly developed over the last decade into a key goal of modern science [6–9]. This chapter is aimed at the observational part of this effort and, in particular, the use of Type Ia Supernovae (SNe Ia) to probe the expansion history. (We do not tackle the theoretical possibilities for explaining the cosmic acceleration in any great detail; excellent reviews of these can be found elsewhere [e.g., 4].)

Type Ia Supernovae (SNe Ia) are a violent endpoint of stellar evolution, the result of the thermonuclear destruction of an accreting carbon–oxygen white dwarf star approaching the Chandrasekhar mass limit, the maximum theoretical mass that a

white dwarf star can attain before the electron degeneracy pressure supporting it against gravitational collapse, is no longer of sufficient strength. As the white dwarf star gains material from a binary companion and approaches this mass limit, the core temperature of the star increases leading to a runaway fusion of the nuclei in the white dwarf's interior. The kinetic energy release from this nuclear burning – some 10^{44} J – is sufficient to dramatically unbind the star. The resulting violent explosion and shock wave appears billions of times brighter than our Sun, comfortably outshining the galaxy in which the white dwarf resided.

Remarkably, SNe Ia are also extraordinary examples of a class of objects known as standard candles, objects with a uniform intrinsic brightness. For SNe Ia, this homogeneity is presumably due to the similarity of the triggering white dwarf mass (i.e., the Chandrasekhar mass, $\sim$1.4 solar masses or $M_{\odot}$) and consequently the amount of nuclear fuel available to burn. This makes SNe Ia the best (or at least most practical) example of "standard candles" in the distant universe, objects to which a distance can be inferred from only a measurement of the apparent brightness on the sky. This allows them to be used to directly trace the expansion rate of the universe.

In this chapter, I will introduce the framework within which SN Ia observations can be interpreted and show how they can be used to constrain the cosmic expansion history. In particular, I will concentrate on the potential systematic issues that could affect their use and show how future cosmological surveys are being designed to mitigate these effects.

2 Context and Basic Concepts

The key problem with understanding dark energy is its very low density – less than 10^{-29} gcm^{-3} – which makes detecting it in a laboratory, let alone studying it in detail, currently impossible. The only reason that dark energy has such an important measurable effect on the physical evolution of the universe is that it is thought to uniformly fill the cosmos. When this low density is integrated over cosmological distances, its effect dominates over that of matter, which is extremely clustered in stars and galaxies. The influence of dark energy can therefore only be observed over cosmological scales, which in turn makes astronomy the only experimental field currently capable of making headway in studying it.

Although there has been much excitement over the last decade, cosmic acceleration is neither a new nor novel concept. Its history can be traced back to the development of the theory of GR, and the idea has re-emerged several times in the intervening century [for a "pre-1998" review see 10]. At the time of the publication of GR, contemporary thinking indicated that the universe was a static place. Einstein perceived that solutions to the field equations of GR did not allow for these static solutions where space is neither expanding nor contracting but rather is dynamically stable. The effects of gravity in any universe containing matter would cause that universe to eventually collapse. Hence, Einstein famously added a repulsive "cosmological constant" term to his equations – Λ.

This cosmological constant has the same effect mathematically as an intrinsic energy density of the vacuum with an associated pressure. A positive vacuum energy density implies a negative pressure (and vice versa). If the vacuum energy density is positive, this negative pressure will drive an accelerated expansion of empty space, acting against the slowing force of gravity. Hence, static universe solutions in GR could now be permitted, at least in principle. Following observations in the late 1920s that the universe was not a static place but instead expands with time, the perceived need for a Λ term in GR was removed. Einstein famously remarked in his later life that modifying his original equations of GR to include Λ was his "biggest blunder."

Despite Einstein's retraction of Λ, in the early 1990s it was realized that, in fact, a cosmological constant could potentially explain many puzzling observational effects in astronomical data. Many cosmologists were disturbed by the low matter density implied by observations of the large-scale structure of the universe – if $\Omega_{\mathrm{M}} < 1$, where was the rest of the matter–energy? Was the universe non-flat or was the interpretation of the observations at fault? The apparent ages of globular clusters were another puzzle, seemingly older than the accepted age of the universe in the then standard cosmological models. This indirect evidence generated a renewed interest in the cosmological constant, which could explain many of these inconsistencies [e.g., 11–13]. However, the first direct evidence did not come until a few years later with observations of SNe Ia.

2.1 Cosmological Framework

In the solutions to Einstein's field equations of GR known as the Friedmann–Lemaitre–Robertson–Walker (FLRW) metric, the universe is described as homogeneous and isotropic, possibly expanding or contracting, and filled with a perfect fluid, one that can be completely characterized by an equation of state w, with an energy density ρ and an isotropic pressure p ($w = p/\rho$). In these solutions, the growth of the universe over time is parametrized by a dimensionless scale factor parameter $a(t)$, essentially describing how the universe "stretches" over time, defined so that at the present day $a = 1$. The equations which govern the expansion are known as the Friedmann equations

$$\frac{\ddot{a}}{a} = -\frac{4\pi G}{3}\left(\rho\left(a\right) + 3p(a)\right) \tag{1}$$

and

$$\left(\frac{\dot{a}}{a}\right)^2 \equiv H^2\left(a\right) = \frac{8\pi G\rho\left(a\right)}{3} - \frac{k}{a^2}\,. \tag{2}$$

The left-hand side of this second equation is the Hubble parameter $H(a)$, which measures the relative expansion rate of the universe as a function of a. Despite a

contentious history, the present-day value of H, the Hubble constant H_0, is generally agreed to be close to $70\,\mathrm{km\,s^{-1}\,Mpc^{-1}}$ using a wide variety of different techniques [e.g., 14]. The right-hand side of (2) determines the expansion rate from the matter–energy contents of the universe. $\rho(a)$ describes the evolution of the mean density of each of the different components of the universe – baryonic matter, dark matter, radiation, neutrinos, dark energy, etc. (G is Newton's gravitational constant). The effect of spatial curvature parametrized by k: $k = 0$ indicates a flat universe.

The density of each component, ρ, evolves with the scale factor a as

$$\rho\,(a) \propto a^{-3(1+w)}\,, \tag{3}$$

with w the (constant) equation of state of each given component.

More conveniently, each of the different components of ρ can be written in terms of energy density parameters Ω defined as a fraction of the "critical energy density" ρ_c, the current energy density of a flat ($k = 0$) universe

$$\Omega \equiv \frac{\rho}{\rho_c} = \frac{8\pi G\rho}{3H^2}\,. \tag{4}$$

Non-relativistic matter has an equation state of $w_\mathrm{M} = 0$. From (3), its energy density Ω_M will be diluted as the universe expands as a^{-3} or by the volume. Ultrarelativistic matter, such as radiation and neutrinos, has $w_\mathrm{rad} = 1/3$. Its energy density Ω_rad is diluted more quickly by the expansion than matter as a^{-4}, decreasing faster than a simple volume expansion as radiation has momentum and therefore a wavelength, stretched by a factor of a. The final component Ω_DE, dark energy, must have a strong negative pressure to explain the observed cosmic acceleration and hence a negative (but not precisely known) w. Equation (2) is then written as (in a flat universe with $k = 0$)

$$H^2\,(a) = H_0^2\left[\Omega_\mathrm{M}a^{-3} + \Omega_\mathrm{rad}a^{-4} + \Omega_\mathrm{DE}a^{-3(1+w)}\right]\,, \tag{5}$$

where w is now the equation of state of only the dark energy component. Here w is assumed constant; for a non-constant w, the final term is replaced by

$$\Omega_\mathrm{DE}\exp\left(3\int_a^1 \frac{da'}{a'}\left[1 + w\left(a'\right)\right]\right)\,. \tag{6}$$

The expansion history of the universe is therefore a "competition" between these different components (Fig. 1). At early times, from around 3 s after the Big Bang until an age of 50,000 years (a cosmological redshift of ∼3,500), the universe was dominated by radiation. As the universe expanded and the radiation energy density dropped off as a^{-4}, the universe entered a matter-dominated era, where the gravitational attraction due to matter caused a period of deceleration. The energy density due to matter falls as a^{-3}, and at an age of about 9 billion years (a redshift of ∼0.45)

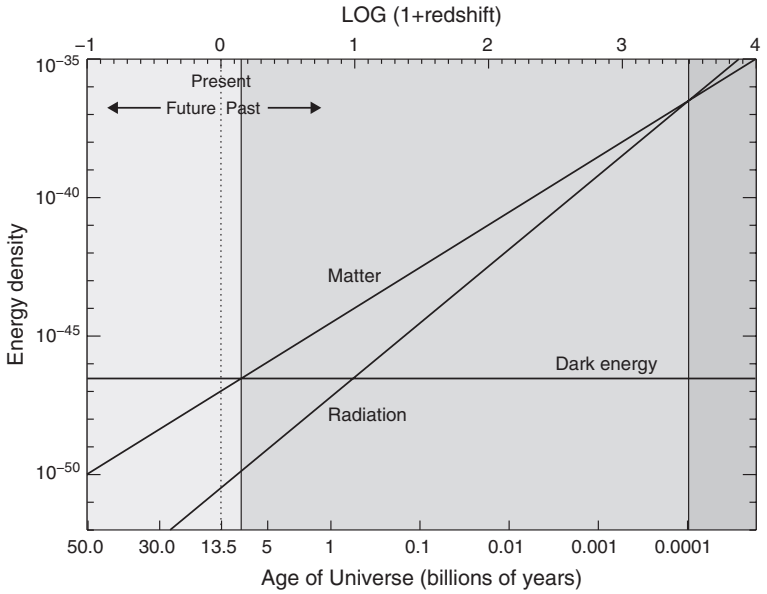

Fig. 1 The importance of the different components of the energy density of the universe as a function of the age of the universe and cosmological redshift for a flat universe. The three epochs discussed in the text are in different shades of *gray*. The early universe, at $z > 3{,}500$, is radiation dominated. Between $0.45 < z < 3{,}500$ is a matter-dominated era, and at $z < 0.45$ the universe is dark energy dominated

the effect of dark energy became dominant over that of gravity (although the effects of dark energy can be observed well before this redshift). Cosmic acceleration is, therefore, a relatively recent phenomenon in the expansion history of the universe, as dark energy was not important in terms of the expansion history at early times.

For the dark energy density term, the "simplest" solution is a cosmological constant, mathematically identical to a vacuum energy with a negative pressure exactly equal to its energy density unchanging with time: $w = -1$. This is equivalent to the Λ term introduced into GR by Einstein, and for that reason dark energy is often denoted by that term. In this case the expansion properties of a universe containing dark energy can be described by three parameters: w, $\Omega_{\rm DE}$, and $\Omega_{\rm M}$ (one parameter fewer if the universe is assumed flat and $\Omega_{\rm DE} + \Omega_{\rm M} = 1$). However, attempts to calculate the vacuum energy density from the zero-point energies of quantum fields result in estimates that are many orders of magnitude too large – a challenge to theories of fundamental physics.

Alternatively to vacuum energy, dark energy may be a scalar energy field of unknown physical origin which varies over both time and space, either decreasing or increasing in energy density, the latter leading to a "big rip" eventually tearing apart all structure. In these cases there is no a priori reason to assume that w is unchanging with redshift and many reasons to think that it is not.

The variety of possibilities to explain the cosmic acceleration make comparisons between observations and theory challenging. Ideally, the energy density of dark energy would be experimentally measured smoothly as a function of time, but in practical terms this is not yet possible. Instead, measuring $w(a)$ requires a parametrization of its form with a. The simplest is to assume w is constant: experiments then measure some average value $\langle w \rangle$. This is particularly valuable for assessing whether cosmic acceleration is consistent with vacuum energy (the cosmological constant): Is $\langle w \rangle$ consistent with -1? However, it is not particularly well motivated for other models of dark energy where w is expected to change with time.

For these "varying w" models, more complicated parametrizations should be used. Many simple, but useful, "two-parameter" parametrizations have been suggested with a linear dependence on either a (or redshift, z). The form $w(a) = w_0 + w_a(1 - a)$ is often used [15]. Other more general and complicated parametrizations are clearly possible [e.g., 16], including a principal component approach where $w(a)$ is measured over discrete intervals [17]. Other model-independent approaches such as direct reconstruction have also been examined [e.g., 18] and tested against real data [e.g., 19]. Each approach has advantages and drawbacks. Simpler parametrizations are easier to measure observationally, but harder to compare with models other than Λ. More complicated parametrizations clearly tend to result in noisier measurements.

As a final point, it should be noted that this framework is only relevant in the context of the FLRW metric and solutions to GR. If, instead, cosmic acceleration is an artifact or an indication of problems with GR, then this concept of w becomes meaningless. Typical approaches along these lines involve changes to the Friedmann equation (1) and (2) and the evolution of $a(t)$.

2.2 Distance Determination: The Standard Candle Method

Having established the simple framework necessary to measure dark energy, we now discuss how this can be achieved using distance estimation techniques. The principle underlying the use of standard candles to constrain the cosmological parameters through the observational effects of dark energy is to measure the expansion history $H(a) \equiv \dot{a}/a$ and compare with (5). The scale factor a is easy to measure via an object's redshift, z. When astronomical objects are observed, the photon wavelengths of the radiation that they emit are stretched ("redshifted") by the expansion of the universe by a factor $1/a = 1 + z$. The rate of change of a, $\dot{a}$ is more difficult (time is not a measurable!). Instead, distances to objects as a function of redshift are used, which are themselves intimately related to the expansion history. The comoving distance d (the distance between two points measured along a path defined at the present time) to an object at a cosmological redshift z is

$$d = \int_0^z \frac{c}{H(z')} \mathrm{d}z' = \frac{c}{H_0} \int_0^z \frac{\mathrm{d}z'}{\sqrt{\Omega_\mathrm{M} (1 + z')^3 + \Omega_k (1 + z')^2 + \Omega_\mathrm{DE} (1 + z')^{3(1+w)}}} , \tag{7}$$

where $H(z)$ is the Hubble parameter from (5), and the equation is written in terms of z rather than a. Related to this comoving distance are a variety of other distance definitions depending on the manner in which the distance measure is made. In particular, for SNe Ia the luminosity distance d_L is particularly useful:

$$d_L \equiv d(1+z)\,. \tag{8}$$

This luminosity distance can be *independently* estimated for an object of known intrinsic bolometric luminosity L (a standard candle) from an observation of the bolometric flux density f of the same object quite trivially as

$$d_L = \sqrt{\frac{L}{4\pi f}}\,. \tag{9}$$

The power of distance measures is clear: when L, f, and z are all known from measurements of a set of astrophysical objects, the only remaining unknowns in (7), (8), and (9) are the cosmological parameters. Thus, measuring a large set of astrophysical objects distributed in redshift which are known to be standard candles (such as SNe Ia) can directly measure parameters of interest and trace out the expansion history via the distance–redshift relation, traditionally on a Hubble diagram. In practice, even a knowledge of the absolute luminosity L is not required. Instead, *relative* distances between local and distant standard candles are sufficient, which has the considerable advantage of removing any dependence on H_0.

The size of the variation in the apparent magnitude[1] of a standard candle versus redshift for different cosmological models is shown in Fig. 2. For a simple measurement of $\langle w \rangle$, the "sweetspot" region is around $z = 0.6$ where the differences between various models are the largest, and the redshift is still small enough that high-quality observational data can be obtained. Above $z = 1$, the relative effect of a change in w in terms of apparent magnitude difference from that at $z = 1$ is very small: at these epochs the universe was decelerating and dark energy had only a minor influence on its evolution. Clearly, when trying to measure $w(a)$, samples of standard candles are required across the entire redshift range: the problem is quite degenerate if only a limited range in redshift can be observed. Figure 2 shows the variation assuming a simple linear function in $w(a)$.

A closely related technique to standard candles uses a different distance measure and the concept of "standard rulers," objects of known dimensions rather than known luminosity. Such sizes can be compared to the angular diameter distance d_A, the ratio of an object's (transverse) physical size to its angular size. It is related to the luminosity distance d_L as $d_A = d_L/(1+z)^2 = d/(1+z)$ and can probe the expansion history in a very similar way as standard candles. The method of measuring

[1] An astronomer's unit defined as $-2.5\log(f)$+constant. Note that smaller magnitudes represent brighter fluxes!

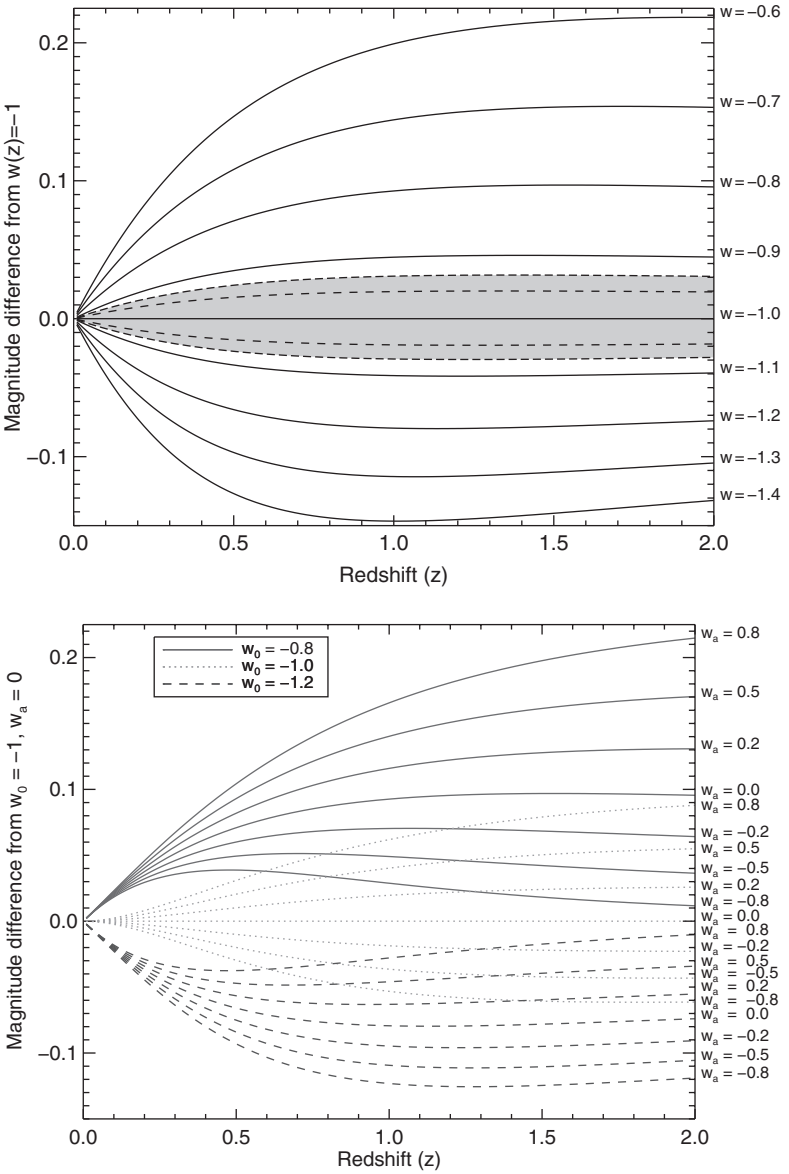

Fig. 2 The predicted variation in the apparent magnitude of a standard candle versus redshift for various cosmological models. In the *top frame* are different models assuming a constant equation of state, for $w = -0.6$ to $w = -1.4$. The current best constraints in $\langle w \rangle$ are shown in the *gray shaded* area. The upper *dashed–dot line* shows the constraints including systematic errors and the *dashed line* just the statistical error. The *bottom frame* is the same plot, but assuming a variable w according to $w(a) = w_0 + w_a(1 - a)$

baryon acoustic oscillations in the galaxy power spectrum, for example, exploits this idea (see Sect. 3.4). Generically, distance–redshift relations $d(z)$ provide very strong constraints on dark energy as they directly track the expansion history.

2.3 Type Ia Supernovae: A Brief Primer

One of the best standard candles known is Type Ia Supernovae, SNe Ia. Though an intimate knowledge of the physics of SNe Ia is not necessary for cosmological applications, it is extremely helpful in understanding the theoretical reasons as to why SNe Ia are such good standardized candles and in understanding the types of systematics that may affect the analysis.

The classification scheme for SNe – Ia, Ib, Ic, II, etc. – is mostly historical accident. Type I SNe were originally those events which did not show hydrogen in their spectra; Type II SNe have prominent H lines. The H-free Type I events were further sub-divided over time: Type Ia show strong Si absorption, Type Ib have no Si but instead He absorption, and Type Ic have no H, He, or Si. All SN types *except* SNe Ia are believed to be the result of the catastrophic core collapse of massive $>$8–10$M_\odot$ stars.

SNe Ia have a different physical mechanism, the result of the thermonuclear destruction of a carbon–oxygen (C–O) white dwarf star residing in a binary system, i.e., with a nearby companion star. Having gained material from this companion via accretion, the mass of the white dwarf star becomes greater than that which can be supported by the electron degeneracy pressure of the white dwarf, at which point the core temperature of the white dwarf increases and C burning ensues in a sub-sonic deflagration. This C fusion raises the temperature further, an increase which cannot be regulated by the white dwarf star, where degeneracy pressure is independent of the temperature. The burning C fusion flame then accelerates into a supersonic detonation [20, 21] and a SN is the result.

Many details of the nature of the SN Ia explosion are still unclear, in particular the exact role of detonation versus deflagration. However, once the explosion has occurred, the resulting observed light curve – the luminosity evolution of the SN as a function of time – is broadly driven by relatively well-understood nuclear physics. The light curve is powered by the radioactive decay of ^{56}Ni, produced during the second or so of the SN explosion, into ^{56}Co, with a half-life of $\sim$6 days, and then by ^{56}Co into ^{56}Fe with a half-life of $\sim$77 days [e.g., 22], a process that can be confirmed observationally using line ratios in the late-time SN Ia spectra [23]. This radioactive decay deposits energetic gamma rays into the SN ejecta, which is heated and radiates thermally to produce the light curve that we observe. The mass of ^{56}Ni produced, $M_{\rm Ni}$, is therefore the primary determinant of the peak brightness of the SN event. Observations indicate that for normal objects, $M_{\rm Ni}$ span the range 0.4–0.9$M_\odot$, with a typical value of 0.6$M_\odot$. Photometrically, SNe Ia rise to maximum light in a period of approximately 20 days, followed by a rapid decline of about three magnitudes in the first month following maximum light and approximately one magnitude per month thereafter.

Though this consensus of an exploding near-Chandrasekhar mass C–O white dwarf star residing in a binary system is seldom seriously debated, the exact configuration of the progenitor system is more controversial. The companion star to the progenitor white dwarf could be a second white dwarf star ("double degenerate") or a main-sequence or giant star ("single degenerate"). Evidence from observations or theory for and against these two possibilities is ambiguous. These uncertainties are some of the biggest drawbacks of the SN Ia technique – in the absence of any theoretical guidance, it must be assumed that any variation can be empirically controlled (see Sect. 3).

Theoretical modeling of a SN Ia explosion is a complex problem, requiring the interior physics of the exploding white dwarf star to be related to what is finally observed: the light curves and spectra. This must be achieved by radiative transfer calculations, an unsolved problem in many astrophysical applications; SNe Ia are no exception. Unlike most astrophysical objects, SNe Ia contain no hydrogen, and therefore the opacities are always dominated by electron scattering (in the optical) or by a vast number of atomic lines (in the ultraviolet) making detailed predictions more challenging. The radiation transport in SNe Ia is non-local and the methods used in models of stellar atmospheres need refinement. The deposition of energy from the light curve and the explosion itself are also likely to be non-symmetrical. Given these complications, much of our understanding of SNe Ia is currently observationally motivated, though recent theoretical progress is now starting to provide theoretical insight [24].

2.4 Discovery of the Accelerating Universe

Type Ia Supernovae (SNe Ia) are apparently ideal as standard candles – they are bright, uniform, and possess a convenient approximately month-long duration during which they can be found and observed. This makes them extremely observationally attractive and practical as calibrateable standard candles, a realization that goes back many decades [25]. Yet, for many years following the realization of this potential, finding distant events in the numbers required for meaningful constraints was a considerable logistical and technological challenge. Years of searching were required to discover only a handful of distant SNe Ia [e.g., 26, 27]. The field only came of age through improving technology: the advent of large format CCD cameras on 4-m class telescopes, capable of efficiently scanning large areas of sky, and the simultaneous development of sophisticated image processing routines and powerful computers capable of rapidly analyzing the volume of data produced.

The substantial search effort culminated in the late 1990s when two independent surveys for distant SNe Ia [27, 28] made the same remarkable discovery: the high-redshift SNe Ia appeared about 40% fainter – or equivalently more distant – than expected in a flat, matter-dominated universe [29, 30, see Fig. 3]. This indicated that the expansion of the universe had been speeding up over the last $\sim$5–7 Gyr, providing compelling direct evidence for an accelerating universe. When these

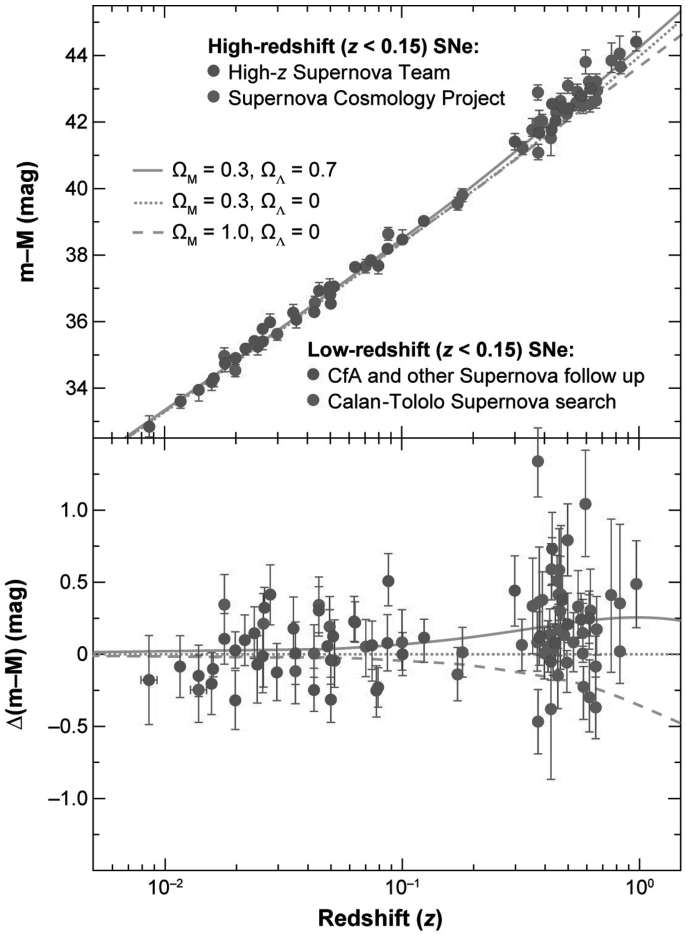

Frieman JA, et al. 2008.
Annu. Rev. Astron. Astrophys. 46:385–432

Fig. 3 The original "discovery data" which directly indicated the accelerating universe. This is the original Type Ia Supernovae Hubble diagram compiled from data taken by the Supernova Cosmology Project [30] and the High-*z* Supernova Search Team [29]. The *lower panel* shows the residuals in the distance modulus relative to an open universe. The SNe Ia lie above and are inconsistent with (fainter than) the non-accelerating universe lines. Reprinted, with permission, from the Annual Review of Astronomy and Astrophysics, Volume 46, © 2008 by Annual Reviews `www.annualreviews.org`

observations were combined with analyses of the cosmic microwave background, a consistent picture emerged of a spatially flat universe dominated by a "dark energy" responsible for ∼70–75% of its energy, opposing the slowing effect of gravity and accelerating the universe's rate of expansion.

Since these original observations, the number of cosmologically useful SNe has dramatically increased. The next section discusses how SNe are typically used in

a cosmological application and shows the latest results from these next-generation samples.

3 Cosmological Applications

Despite the claim that SNe Ia are standard candles, this is in fact a hugely oversimplified statement. SNe Ia possess approximately a factor of two variation in their "raw" peak brightnesses – limiting their usefulness in cosmological applications. The key astrophysical development in the cosmological use of SNe Ia was the realization that their luminosities could be further homogenized, or standardized, using simple empirical techniques and correlations between SN luminosity and other variables. As such, SNe Ia are *standardizable*, rather than standard, candles. There are two relationships commonly used to standardize SN Ia luminosities, discussed in the next section.

3.1 Standardization

The most well-known relationship is the classic light-curve width–luminosity relationship (WLR), the "Phillips relation" [31]. Raw SN Ia peak luminosities are strongly correlated with the width of the SN light curve – intrinsically brighter SNe Ia typically have wider (i.e., slower declining) light curves. Equivalently, SN Ia light curves can be described using a "stretch" parameter s [27], which stretches or contracts a template SN light curve to match an observed light curve: high-stretch SNe have wider and brighter light curves than average, and low-stretch SNe have narrower and fainter light curves.

The physical origin of this relationship is not universally agreed upon, but must be related to the mass of ^{56}Ni, $M_{\rm Ni}$, synthesized in the SN Ia explosion. Clearly, if more ^{56}Ni is synthesized, the SN will have an increased peak luminosity, and therefore a higher temperature. As the SN ejecta remain optically thick for several months following the SN explosion, the width of the light curve is therefore related to the timescale for photons to escape from the ejecta by diffusion. Therefore, the WLR could be explained if brighter SNe Ia have higher effective opacities, κ, and hence a longer diffusion time, which scales as $k^{1/2}$, meaning the photons take longer to escape and a broader light curve is the result.

Several related physical mechanisms have been postulated to explain the WLR [for an excellent summary, see 32]. The first is a simple temperature effect [e.g., 33]: SNe Ia with a larger $M_{\rm Ni}$ have higher temperatures, leading to more radiation at shorter wavelengths, in the ultraviolet rather than the optical. As line opacity is substantially higher in the blue, κ should increase with an increasing $M_{\rm Ni}$. The second mechanism is related to ionization state [e.g., 34, 35]: the diffusion time becomes shorter when ultraviolet photons are able to fluoresce to longer wavelengths and escape, via interactions with Fe-group elements. This fluorescence is more efficient in singly ionized species, which are more common in cooler (smaller $M_{\rm Ni}$) SNe.

A third mechanism is simply related to the ejecta composition [36]: A larger $M_{\rm Ni}$ implies more Fe-group elements and therefore larger opacities.

More recent work [32] suggests that while present, these three effects are of secondary importance, and the WLR is instead driven primarily by the blanketing from Fe II/Co II lines which appear earlier in cooler SNe with smaller $M_{\rm Ni}$, and therefore produce a faster decline rate. Contemporary models are now capable of qualitatively reproducing the observational WLR [32, 24].

The second, and less well-understood, relationship is between the SN Ia luminosity and the SN color – intrinsically brighter SNe Ia typically have a bluer optical color than their fainter counterparts [e.g., 37]. Here, color is measured as the difference in magnitudes (or ratio of fluxes) in the B[2] and V bands. Naively, this is exactly the sense that would be expected from the dimming effect of dust – dust along the line of sight to distant SN events should both redden *and* dim their spectral energy distributions (SEDs). However, there is a major complicating factor. If the dust in distant galaxies which host SNe Ia is assumed to be the same as that present in the Milky Way, the result should be a relationship between SN color and luminosity much steeper than that observed. Multiple studies show that the Milky Way value for the ratio of total to selective extinction in the rest-frame B-band (R_B) of 4.1 is not consistent with that found when analyzing SNe Ia, with all evidence pointing to an effective $R_B < 4.1$: the color corrections on SN Ia are *incompatible with known galactic dust properties* [e.g., 39–41].

This suggests one of three possibilities. The first is that dust in galaxies which host SNe Ia is radically different to dust in the Milky Way. However, observations of quasars behind foreground galaxies can be used to probe extinction laws in other galaxies and show little evidence for this effect [42]. A second possibility is that the circumstellar dust surrounding the SN Ia progenitor white dwarf may play an important role [43]. Finally, there may be an additional intrinsic relationship between SN color and luminosity that does not correlate with light-curve shape. Interestingly, recent SN simulations do show evidence for intrinsic color–luminosity relationships in the same sense as that observed in the data [24].

So far, stretch and color are the only two photometric parameters that have been found to correlate with SN Ia luminosity, and nearly all cosmological analyses exploit these relationships, albeit in varying forms. The two relationships are shown in Figs. 4 and 5 using a sample of modern SN Ia data. These relationships can be applied to observed peak magnitudes m and take the form

$$m_{\rm corr} = m + \alpha\,(s-1) - \beta\mathcal{C}\ , \tag{10}$$

where the stretch–luminosity is parametrized by α, and the color–luminosity relationship is parametrized by β. Applying these, or similar, calibrating relationships

[2] The B-band is an optical "filter" centered at ∼450 nm and with a full width of ∼100 nm. The V-band is redder at ∼550 nm. See [38] for typical bandpasses assumed for this and other standard optical filters.

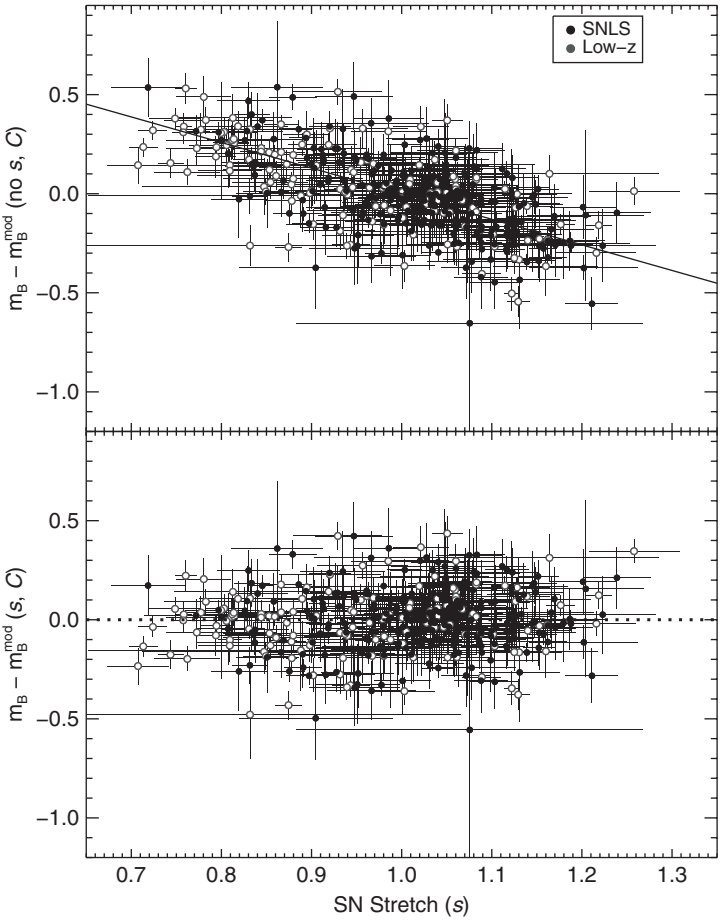

Fig. 4 The relationship between SN Ia luminosity and light-curve stretch. The *upper panel* shows the relationship, while the *lower panel* shows the trend between luminosity stretch after the best-fit relationship (*solid line* in *upper panel*) has been removed from the data. The *open circles* show data at low redshift, and the *filled circles* show data at high redshift

to SN Ia measurements provides distance estimates precise to ∼6–7% or 0.12–0.14 magnitudes, using various independent techniques [44–46].

3.2 Light-curve fitting

In nature, SNe Ia do not come neatly packaged in the form required for cosmological analyses. SNe are not usually observed exactly at maximum light, where they are best calibrated as standard candles, and the redshifting of their SEDs requires their observed fluxes be *k*-corrected back to the rest frame before they can be used in a cosmological context. Therefore, light-curve fitting is a critical component of a

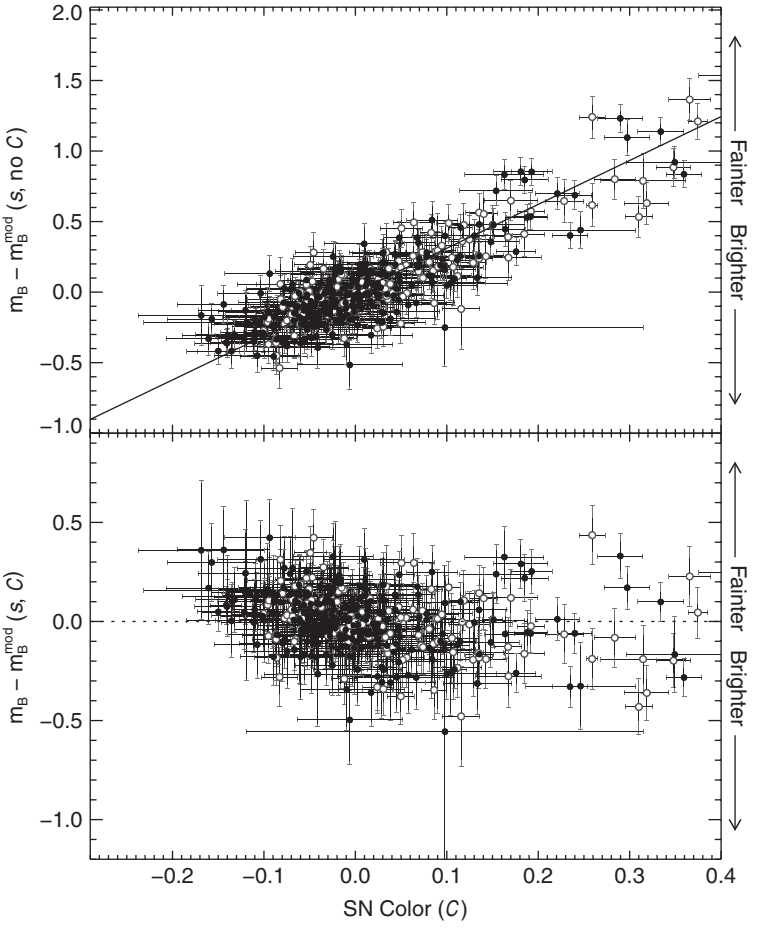

Fig. 5 As Fig. 4, but for SN C instead of stretch

cosmological analysis. This requires modeling of the SN light curves and spectra, and the importance of light curve fitting can be seen by considering the large number of methods described in the literature: a partial sample includes MLCS/MLCS2k2 [47, 44], stretch [27, 48, 49], Δm_{15} [50, 51], BATM [52], CMAGIC [53], SALT2 [45], and SiFTO [46]. These approaches vary considerably. For some SNe they produce very different results, but when a reasonably large sample is considered, the overall results are quite similar [54, 46].

The distinction between light-curve fitters and distance estimators is often not made explicit in the literature. The majority of the published packages are light-curve fitters, with the exception of MLCS/MLCS2k2 and BATM. A light-curve fitter attempts to find the best fit to a given set of observed SN Ia photometry. The parameters of this fit are then usually converted into a distance estimate, but technically this step is not part of the light-curve fit. A distance estimator attempts to find the distance directly rather than trying to obtain the best fit to the data. In both cases, only a relative distance is required.

The advantage of a distance estimator is that the output is what is desired for *most* applications of SN Ia data. Therefore, the products of such an analysis are simpler to use, and in principle such an approach may do a better job extracting the information directly relevant to this purpose. Their primary disadvantage is that, by their nature, distance estimators must use distance information in their training, usually in the form of residuals from the best-fit Hubble relation. This makes it difficult to include very low-redshift SNe which are not in the smooth Hubble flow and high-redshift data since here the residuals are strongly dependent on the cosmological model. To use such data properly, it is necessary to re-train the model from scratch for every value of the cosmological parameters one evaluates, which will be extremely computationally expensive. Therefore, in practice, light-curve fitters have access to a larger data set for training purposes. Neither approach is a priori obviously superior, though the advantages of incorporating data from a range of redshifts in the training does make light-curve fitters compelling. In particular, light-curve fitters are able to make use of the blue/UV part of the SN Ia SED by using high-redshift SN data, where the rest-frame UV is redshifted into optical bandpasses. Using this data in the model training can allow a drastic improvement in the color measurement for the most distant SN events. Depending on the data set, both light-curve fitters and distance estimators can be used with a typical precision of ∼6–10%.

The goal of both light-curve fitters and distance estimators is to reduce each SN Ia to a set of parameters that can then be used in cosmological fits. Here, we concentrate on light-curve fitters, though the same basic principles apply to distance estimators. A light-curve fitter such as SALT2 or SiFTO estimates, for each SN, its peak magnitude in some rest-frame passband, a measure of its light-curve shape and a measure of its color. Here we use the peak magnitude in the rest-frame B-band, m_B, the stretch s, and the $B-V$ color at the time of maximum light in the rest-frame B-band, $\mathcal{C}$. In principle, any rest-frame passband and color could be used; in practice the chosen passband should always correspond to a part of the SN Ia SED that is directly measured at all redshifts under study, which currently makes the B-band the most practical.

An integral part of any light-curve fitter (or distance estimator) is the k-correction. This converts a flux in an observed passband (e.g., r) into one in a rest-frame passband, in this case one common to all SNe (e.g., B). Given an SED model of the SN Ia ϕ_{SN}, parametrized by wavelength λ and epoch t, the rest-frame apparent magnitude m of a SN in filter B with a total system response T_B is given by

$$m_B = -2.5 \log_{10} \left[\frac{\int \phi_{\mathrm{SN}}(\lambda,t)\, T_B(\lambda)\, \lambda D\lambda}{\int \phi_{\mathrm{REF}}(\lambda)\, T_B(\lambda)\, \lambda D\lambda} \right] . \tag{11}$$

where ϕ_{REF} is the SED of some known and calibrated photometric reference SED, which places the measurement onto a known photometric system. This reference SED is classically chosen to be the A0V star, α-Lyrae or Vega.

In practice, experimentally Vega is a poor choice of flux reference standard – at an apparent magnitude of zero, it is far too bright to be observed by most telescopes, saturating CCD detectors. Calibration is, therefore, performed using observations of secondary stars that have previously been to a particular system, e.g., the Landolt

system [55], close to a Vega-based system. Unfortunately, Vega is quite a blue star and is unrepresentative of most of the secondary stars that have been chosen for observational calibration purposes. Modern precision calibration often, therefore, makes use of alternative flux reference SEDs to Vega, such as that of BD 17° 4708, which are fainter, have been calibrated to a higher precision, and have colors more similar to that of the secondary standards.

For the same SN observed in a passband r at a heliocentric redshift $z_{\rm hel}$, the observed apparent magnitude m_r is

$$m_r = -2.5 \log_{10} \left[\frac{1}{1+z_{\rm hel}} \frac{\int \phi_{SN}\,(\lambda,t)\, T_r\,(\lambda/\,(1+z_{\rm hel}))\,\lambda D\lambda}{\int \phi_{\rm REF}\,(\lambda)\, T_r\,(\lambda)\,\lambda D\lambda} \right] . \tag{12}$$

The k-correction is then defined as the difference between the two, namely

$$kc = m_r - m_B\ . \tag{13}$$

Thus, a conversion between observed and rest-frame magnitudes can be achieved.

These equations have two important implications. First, the SED of a typical SN Ia must be well known, over the entire light curve or phase for which there are photometric observations. SNe Ia demonstrate significant spectral evolution with time, and thus many observed SN Ia spectra are required to construct a spectral template suitable for light-curve fitting. Considerable work over the last decade has ensured that these templates are now generally available [56, 57]. The second implication is that a well-measured photometric reference SED must exist, for which magnitudes in a given passband must be known (see discussion above), allowing synthetic photometry to be performed for comparison to observed measures. Any uncertainty in which this SED is calibrated will directly impact as a systematic in the subsequent use of the peak magnitudes (see Sect. 4.1).

The light-curve fit is then a simple χ^2 minimization between the observations and synthetic magnitudes calculated according to (12), producing a peak magnitude, stretch, and color (together with their errors and covariances) which can be carried forward, for each event, to the cosmological parameter estimation stage, described in the next section.

3.3 Cosmological Parameter Estimation

A typical SN Ia cosmological fit minimizes an equation of the form

$$\chi^2 = \sum_N \frac{\left(m_B - m_B^{\rm mod}\,(z;\alpha,\beta,\mathcal{M}_B;\Omega_{\rm M},\langle w\rangle,...)\right)^2}{\sigma_{\rm stat}^2 + \sigma_{\rm int}^2}\ , \tag{14}$$

where we only include statistical errors for clarity. $\sigma_{\rm stat}$ is the total identified statistical error and includes uncertainties in both m_B and $m_B^{\rm mod}$, $\sigma_{\rm int}$ parametrizes the

intrinsic dispersion of each SN (see below), and the sum is over the N SNe Ia entering the fit. m_B are the maximum-light SN rest-frame B-band apparent magnitudes output from the light-curve fitter, and $m_B^{\rm mod}$ are the model B-band magnitudes for a SN at a redshift z given by

$$m_B^{\rm mod} = 5\log_{10}\mathcal{D}_L(z) - \alpha(s-1) + \beta\mathcal{C} + \mathcal{M}_B\ , \tag{15}$$

where $\mathcal{D}_L$ is the c/H_0 reduced luminosity distance d_L of (8). The c/H_0 factor in d_L is absorbed into $\mathcal{M}_B$; c is the speed of light. Explicitly, $\mathcal{M}_B = M_B + 5\log_{10}(c/H_0) + 25$, where M_B is the absolute magnitude of a SN Ia in the rest-frame B-band. Neither H_0 nor M_B need be assumed during the fitting process. The α and β nuisance parameters describe the stretch and color–luminosity relationships (Figs. 4 and 5) as described in (10). Any linear variation between SN color and stretch is also allowed for and is absorbed into the α term. The $\sigma_{\rm stat}$ term includes identified statistical errors affecting each SN. This typically comprises the statistical error in m_B from the light-curve fit, the statistical error in $m_B^{\rm mod}$ (essentially $\alpha\sigma_s$ and $\beta\sigma_{\mathcal{C}}$), a peculiar velocity error, the measurement error in each SN redshift projected into magnitude space, the uncertainty from Milky Way extinction corrections applied to m_B, and the covariances between s, $\mathcal{C}$, and m_B, which are correlated for an individual SN. $\sigma_{\rm stat}$ must be updated during the fitting process as α and β nuisance parameters are altered.

The $\sigma_{\rm int}$ term parametrizes the extra dispersion in m_B above and beyond the statistical and model uncertainties required to give a reduced χ^2 of one in the cosmological fits [e.g., 28]. This "intrinsic" dispersion could arise from unidentified sources of error in the analysis, but more likely is due to the imperfect nature of SNe Ia as standard candles – the α and β corrections do not completely eliminate the scatter in the SN Ia magnitudes. As $\sigma_{\rm int}$ may also include contributions from unidentified experimental errors, there is no a priori reason for its value to be the same from SN sample to SN sample.

The best-fitting cosmological parameters can then be found by forming a grid over the parameters of interest and computing the χ^2 of (14) at every point, converting into a probability via $P \propto \exp\left(-\frac{1}{2}\chi^2\right)$, with the proportionality set by normalizing over the grid. The "nuisance parameters" α, β, and $\mathcal{M}_B$ are marginalized over when generating confidence contours in the parameters of interest. Note that $\mathcal{M}_B$ can be marginalized analytically [e.g., 58], but this is not possible for α and β (doing so can bias the values found). These three parameters should not be assumed or fixed in the fit, as the uncertainties in their values need to be propagated.

3.4 Complementarity with Other Probes

Several of the cosmological parameters can, in principle, enter the χ^2 calculation of (14): the matter density $\Omega_{\rm M}$, the energy density of dark energy $\Omega_{\rm DE}$ and its equation of state w, and potentially the amount of curvature in the universe Ω_k. Other

complementary observations are, therefore, useful in conjunction with SNe Ia which place constraints, or priors, on $\Omega_{\rm M}$ (e.g., observations of large-scale structure) or Ω_k (e.g., observations of the cosmic microwave background). At the time of writing, the techniques in common use and therefore most useful are observations of the cosmic microwave background and measurement of baryon acoustic oscillations. We briefly discuss these in turn.

3.4.1 The Cosmic Microwave Background

The cosmic microwave background (CMB) is a nearly isotropic background radiation discovered in the 1960s [59] with a near-perfect black body spectrum, peaking in the radio with a temperature of $\simeq 2.7$ K. The radiation originates from the early universe when the universe was much hotter and denser, and almost entirely ionized – photons and baryons were tightly coupled to each other, opaque to radiation. Some 370,000 years after the Big Bang at $z \sim 1{,}100$, the universe had expanded sufficiently and adiabatically cooled to a temperature near 3,000 K where electrons and protons are able to (re)combine to form neutral hydrogen ("The epoch of recombination"), decoupling the photons and baryons. The photons, free from the baryons, then propagate through the universe and appear as the CMB. As the universe has expanded by a factor of $\sim$1,100 since the epoch of recombination when the CMB was emitted, CMB photons appear considerably less energetic, redshifted into the microwave spectral region.

The CMB is extremely isotropic, but there are small temperature fluctuations of the order of 1/1000th of 1%. Before recombination, any initial density fluctuations, or perturbations, excite gravity-driven sound wave or acoustic oscillations in the relativistic-ionized plasma of the early universe. The matter and radiation are attracted, by gravity, into these regions of high density. A gravitational collapse then follows until photon pressure support becomes sufficient to halt the collapse, causing the overdensity to rebound because of the finite pressure of the gas, generating acoustic waves. These two effects compete to create oscillating density perturbations, driven by gravity and countered by photon pressure. At recombination as the photons are decoupled, those photons originating in overdense regions will appear hotter than average, while those from less-dense regions will appear colder. These small density fluctuations in the universe at that time are, therefore, imprinted directly onto the photons of the CMB, appearing to us as small temperature fluctuations or a temperature anisotropy.

These temperature differences can be "routinely" measured from the CMB power spectrum, the fluctuation in the CMB temperature (anisotropy) as a function of angular scale on the sky. This angular power spectrum of the CMB temperature anisotropy [60, 61, Fig. 6] series of peaks and troughs arises from the gravity-driven acoustic oscillations of the coupled photon–baryon fluid in this early universe. In particular, a strong peak is seen in the power spectrum on an angular scale corresponding to the sound horizon (r_s, the maximum distance sound waves can travel before recombination), where a perturbation crossed this horizon at exactly the time of recombination – the scale that was first feeling the causal effects of gravity at that

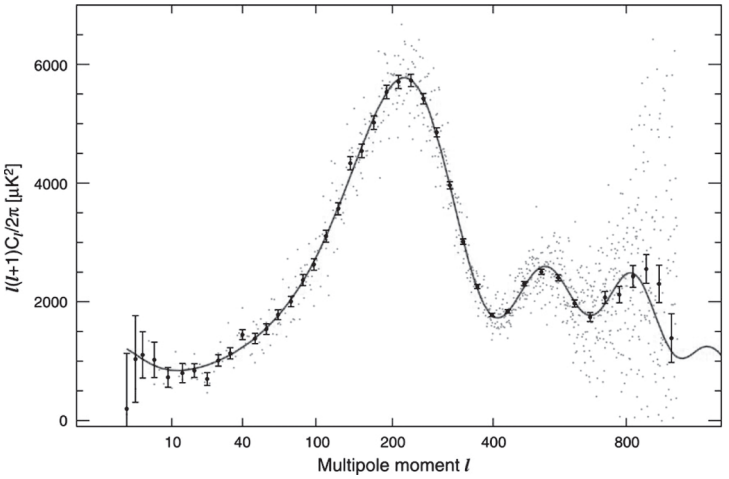

Fig. 6 The temperature anisotropy angular power spectrum from the WMAP-5 data [61]. The small gray dots represent the unbinned data, and the solid points the binned data with $1-\sigma$ error bars. The overplotted line is the best-fit ΛCDM cosmological model. From Dunkley et al. [61], Fig. 2. Reproduced by permission of the AAS

epoch. Smaller scales had been oscillating for longer and manifest as weaker peaks in the angular power spectrum.

A wealth of cosmological information is contained in positions and heights of the series of peaks and troughs [e.g., 62, 63]. The first peak, corresponding to the physical length of the sound horizon at recombination, depends on the curvature of space. If space is positively curved, then this sound horizon scale r_s will appear larger on the sky than in a flat universe; the opposite is true if space is negatively curved. The third peak can be used to help constrain $\Omega_{\rm M}$. However, the CMB by itself provides little direct constraint on dark energy – its role is a significant contribution in constraining Ω_k and $\Omega_{\rm M}$ (as well as the size of the sound horizon) for use in conjunction with other probes.

3.4.2 Baryon Acoustic Oscillations

Baryon acoustic oscillations (BAO) are closely related to the oscillations in the CMB angular power spectrum (Fig. 6). Following recombination, the immediate loss of photon pressure led to a consequent reduction in the effective sound speed of the baryons. The acoustic waves excited by the gravitationally unstable density fluctuations became "frozen" into the matter distribution with a characteristic size equal to their total propagation distance – the sound horizon scale r_s. This r_s can be seen in the power spectrum of the CMB temperature anisotropy, but additionally these sound waves remain "imprinted" in the baryon distribution and, through gravitational interactions, in the dark matter distribution as well. As galaxies (roughly) trace the dark matter distribution, observations of galaxy clustering can uncover this characteristic scale. Making this observation at different redshifts, therefore, allows

this scale r_s to be used as a standard ruler (Sect. 2.2) – just as SNe Ia trace $d(z)$ using $d_L(z)$, BAO measure $d_A(z)$ [e.g., 64, 65].

Power spectra analyses of galaxy redshift surveys contain the acoustic oscillations and are used to measure the cosmological parameters: the conversion of redshifts data into real space requires a cosmology to be assumed, and an incorrect choice will distort the power spectrum with the acoustic peaks appearing in the incorrect places. Observations of the CMB play a critical role here, as this same characteristic scale can be calibrated accurately by observations of anisotropy in the CMB imprinted at the same epoch. This observed, calibrated scale can, therefore, be used as a geometric probe of the expansion history – a measurement at low redshift provides an accurate measurement of the distance ratio between that redshift and $z \simeq 1{,}100$. Spectroscopic redshift BAO surveys can also measure the change of this characteristic scale radially along the line of sight as well as in the transverse direction, in effect a direct measurement of $H(z)$.

Measurements of the power spectra of galaxies are challenging. The oscillations appear as a series of bumps with an amplitude of only about 10%. This is substantially more subtle than the acoustic oscillations observed in the power spectrum of the CMB anisotropies because the impact of baryons on the far larger dark matter component is relatively small. Hence, enormous galaxy spectroscopic redshift surveys covering substantial volumes are required to make a constraining measurement. Photometric redshift surveys could, in principle, also be used and cheaply add hundreds of thousands of galaxies, this comes at the expense of a measurement of $H(z)$ and reduces the ability to measure $d_A(z)$ due to systematic errors and the higher noise of photometric redshifts over spectroscopic measures.

Although using BAOs to measure dark energy with precision requires enormous survey volumes and millions of galaxies, numerical simulations suggest that systematic uncertainties associated with BAO measurements are small – this method is currently believed to be (relatively) unaffected by systematic errors. The physics underlying the standard ruler can be understood from first principles. The main systematic uncertainties that are present in any interpretation of BAO measurements are the effects of nonlinear gravitational evolution and scale-dependent differences between the clustering of galaxies and of dark matter (known as bias). For spectroscopic redshift surveys, redshift distortions of the clustering can also shift the BAO features. However, studies suggest the resulting shift of the scale of the BAO peak in the galaxy power spectrum is 1% or less [e.g., 66].

3.5 Latest Cosmological Constraints

As might be expected, the quantity and quality of SN Ia data have dramatically improved since the original surveys. Dedicated allocations of observing time on 4-m class telescopes, such as the Canada–France–Hawaii Telescope (CFHT) and the Cerro Tololo Inter-American Observatory (CTIO) Blanco telescope, have provided homogeneous multi-color light curves of more than 500 distant SN Ia events over $z = 0.3-1.0$. The principle advances in this redshift range have come from the Supernova Legacy Survey [SNLS; 39] and ESSENCE [54]. At higher redshifts,

above $z = 1$, the *Hubble Space Telescope* has been used to locate ∼25 SN Ia events probing the expected epoch of deceleration [67, 68]. These latter observations also rule out the invocation of "gray dust" to explain the SN data in place of acceleration (see Sect. 4.1).

Lower redshift SN Ia samples are also important – and often neglected. The absolute luminosity of a SN Ia is not known precisely as the distance must be known independent of H_0 and so cannot be used a priori. The SN Ia method instead measures relative distances. Sets of local SNe at $0.015 < z < 0.10$, where the effect of varying the cosmological parameters is small, essentially anchor the analyses and allow relative distances to the more distant events to be measured. (At redshifts lower than $\simeq$ 0.015, the peculiar velocities of the SN Ia host galaxies, or bulk flows, can make the measurement both noisier and biased if not corrected for – see Sect. 4.1). The Sloan Digital Sky Survey (SDSS) SN survey is set to fill in the region from $0.1 < z < 0.3$, and many hundreds of lower redshift SNe Ia in the nearby Hubble flow ($0.03 < z < 0.1$) are either available or upcoming [e.g., 69–73]. The result of these new SN Ia data sets is a comprehensive set of well-calibrated events uniformly distributed from the local universe out to $z > 1$.

The current status of cosmological measurements of dark energy can be seen in Fig. 7 [74]. This uses around 500 SN Ia distributed in redshift from different SN Ia surveys, observations of the CMB from the WMAP-5 data release [61], and BAO measurements from the SDSS [75]. Using this combination of techniques, the latest results show that $\langle w \rangle$ is consistent with -1 with a sub-5% statistical precision. Systematics increase this total error to about 7% (see Sect. 4.2), though it should be cautioned that only systematics from the SN Ia analysis are included in this error estimate. Of particular note is that, at the present time, the BAO measurements provide an almost orthogonal constraint to SNe Ia in $\Omega_M/\langle w \rangle$ space (Fig. 7). Without

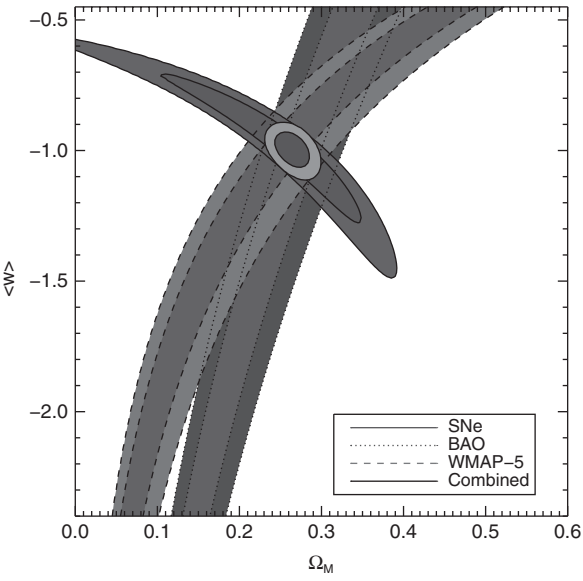

Fig. 7 Latest constraints on the nature of dark energy from SNe Ia and other techniques. The contours show the joint 1σ and 2σ constraints in $\langle w \rangle$ and Ω_M from SN Ia, baryon acoustic oscillations [75], and the cosmic microwave background WMAP-5 results [76]. A flat universe is assumed. The contours show statistical errors only and do not include systematic uncertainties

either the SN Ia constraints or the BAO, our measurement of the equation of state of dark energy would be considerably weakened. This is currently generically true – no single technique can yet place tight constraints on dark energy in isolation.

In the next section, we review the current systematic uncertainties which affect the SN Ia measurement and how these might be improved and reduced with upcoming surveys.

4 Systematics in SNe Ia

Though SNe Ia provided the first direct evidence for dark energy, and still provide the most mature and constraining measurements, there are a number of potential drawbacks to the technique – the apparently simple standard candle concept has several non-apparent difficulties. These difficulties are fundamentally related to the precision required (Fig. 2): detecting departures in dark energy from $w = -1$ requires an extremely sensitive experiment. A 10% difference in w from -1 is equivalent to a change in SN Ia brightness at $z = 0.6$ of only 0.04 magnitudes, or $<4\%$ in flux units, a level of precision perhaps not routinely achieved in astronomy. Therefore, systematic effects must be tightly controlled in any SN Ia experiment.

We discuss two broad classes of systematic error in this section. The first are identified systematics, those which are tractable, can be modeled, and the effects of which directly included in the cosmological fits. The second are the putative and more nebulous astrophysical systematics, related to uncertain configuration and physics of the SN Ia progenitor and explosion.

4.1 Identified Systematics

There are many different sources of identified systematic error in SN Ia experiments. The following is a brief summary of the most important at the time of writing. A full discussion can be found in [77].

Photometric calibration The required calibration of the SN Ia flux data onto a standard photometric system at a 1% accuracy is a challenging task [78] and remains the major source of systematic uncertainty in SN Ia experiments. This calibration must be controlled to the same level in both the high-redshift and low-redshift SN Ia samples. Calibration can be considered to consist of two steps: first, the observations must be standardized onto some photometric system by comparison to stars of known magnitude or flux [55]. Second, it is necessary to convert from this standard system into (relative) fluxes in order to compare SNe at different redshifts (and therefore observed at different parts of their SED). The first set is usually referred to as zero-point uncertainties the second as flux calibration uncertainties, which includes both bandpass uncertainties and uncertainties in the magnitudes of the chosen flux reference in those same bandpasses (see (11) and (12)).

Large, single instrument SN Ia surveys, such as those operating at high redshift, have a clear advantage here: they can devote considerably more effort to internal calibration than is practical for small surveys or those which make use of many instruments. In this regard, the zero-point uncertainty in calibrating to a standard system is usually quite small. Flux calibration uncertainties are more significant. In existing low-redshift surveys, the exact filter bandpasses are often not well measured. Further, calibrating low-redshift and high-redshift SN data onto the same system is a challenge as the observations are made in different filter systems (low-redshift data tend to be observed in the *UBVRI* photometric system, while high-redshift data are in the *griz* system). There are few standard stars with calibrated magnitudes in both systems, making this step one of the most uncertain in the analysis chain.

The color relation of SNe Ia Ideally, all of the measured colors for every SN Ia would be directly used in the distance estimate. In practice, this is difficult as the same rest-frame colors are not measured for all SNe even within the same survey. Therefore, most light-curve fitters make use of empirical relations between different wavelengths to build a single-color parameter for each SN ($\mathcal{C}$). These color relations have statistical uncertainties which are included in the final error budget. A particularly difficult issue relates to the fact that no SN color model perfectly reproduces the observed colors. That is, there is additional scatter in the relation between measurements at different wavelengths that is not explained by the measurement errors, and this intrinsic scatter must be accounted for in the color relations. The error on this scatter is very challenging to constrain and depends strongly on the functional form assumed.

SN Ia model uncertainties Even if all of the other systematics were absent there would still be some uncertainty in the SN Ia model used in the light-curve fitters as it is derived, or trained, from a limited set of data. This uncertainty takes a number of forms, such as errors in the SED (affecting the k-corrections), and errors in the relations that are used to combine different rest-frame colors into the color parameter, $\mathcal{C}$. Encouragingly, in implementations of the light-curve fitters SALT2 and SiFTO where the fitters use the same incidental settings (such as the filter response functions), the resulting fits on the same data are very similar [46]. Nonetheless, some differences do remain, and these should be included as a systematic error in the cosmological analysis.

Comparisons with distance estimators such as MLCS2k2 [44] are more problematic (see Sect. 3.2). Unlike SALT2 or SiFTO, MLCS2k2 explicitly attempts to separate intrinsic and extrinsic SN colors from photometric data, assuming that the extrinsic colors arise purely from dust, and that the remaining intrinsic color not related to the shape of the light curve does not affect the SN luminosity. SiFTO and SALT2 do not make this distinction. The merits of the two approaches depend critically on how well this separation can be performed and how well SN intrinsic color can be predicted by the light-curve shape. The former depends on accurate models of the distribution of extinction with redshift and how they combine with selection effects [54]. If these two conditions are met, then MLCS2k2, by incorpo-

rating additional information beyond SN photometry, may be able to give tighter statistical constraints on SN relative distances. A test of how well this procedure works is to check if the MLCS2k2 prediction of A_V after separation correlates with the residual from the Hubble diagram. Currently available versions fail this test [40], which indicates that, even if the second assumption is correct, the separation is not working correctly. While we fully expect that this situation will be addressed, especially in light of the improved low-redshift data sets that should soon be available, this means that comparing MLCS2k2 fits to SiFTO and SALT2 at the current time is not a useful way to study systematic errors.

Contamination by non-SN Ia Most SNe Ia used in cosmological analyses are spectroscopically typed, giving both a redshift and a firm indication that the object under study is a SN Ia and not some other transient event. Therefore, contamination by non-SNe Ia is expected to be minimal in most analyses. However, some is inevitable, particularly at the highest redshifts where the signal to noise of the confirmation spectra can be quite low. The principal contaminants are expected to be bright SNe Ib and Ic, the population demographics of which we know relatively little, which makes estimating the effects of any contamination difficult and imperfect. Reference [79] takes the approach of and modeling the population of bright SNe Ib and Ic as a Gaussian distribution in magnitude space with some width $\sigma_{\rm bc}$ and a mean offset of $\Delta_{\rm bc}$ from the SN Ia population. For current surveys, the effects on the cosmology are smaller than can be accurately measured, though any bias increases strongly with redshift where observations are larger and the fraction of SNe with more ambiguous spectra with CI 3 increases strongly. This may not be the case in future surveys that, due to their size, may have to rely on photometric rather than spectroscopic typing. Such efforts will require a much more precise understanding of the properties and demographics of SN Ib and Ic if they are to compete with spectroscopic surveys.

Malmquist bias Selection effects in SN Ia surveys, known collectively as "Malmquist bias," can also act as a systematic effect and must be included. At higher redshift, brighter (therefore bluer and higher stretch) SNe Ia will be preferentially discovered and followed spectroscopically, which would lead to a systematic brightening in the Hubble diagram residuals if left uncorrected. Fortunately, modern surveys such as SNLS can be simulated and the magnitude of this effect estimated. Corrections can then be applied directly to the SN Ia magnitudes and the uncertainties in these corrections included as a systematic error. Such simulations are substantially harder to perform on lower redshift surveys, which are not blind, rolling searches as at high-redshift, but instead tend to target known galaxies. This will be rectified in the next few years as a new generation of rolling low-redshift SN searches get underway.

Peculiar velocities The redshift lever arm needed to accurately measure the cosmic expansion requires the use of a local sample, and coherent large-scale local ($z < 0.1$) peculiar velocities add additional uncertainty to the Hubble diagram and hence to the derived cosmological parameters. It is possible to use local data to measure the local

velocity field and hence limit the impact on the derived cosmological parameters by "correcting" the measured redshifts of the local SN Ia host galaxies [80, 81]. Uncertainties in this correction are propagated through the cosmological fits as a systematic uncertainty.

Hubble bubble A related issue is the possibility of a monopole term in the local expansion — a so-called Hubble bubble. Recently, [44] found evidence for such an effect using light-curve fits to nearby SNe Ia. As discussed in [40], this is related to the interpretation of SN colors and the assumption that the relation between SN luminosity and color is well represented by a Milky Way dust law – the same issue is discussed in Sect. 3. The result is that when the same data is analyzed in a framework in which the relation between SN color and luminosity is determined from SN data, no evidence for a Hubble Bubble is seen.

Milky Way extinction correction SN Ia peak magnitudes are corrected for Milky Way extinction using the maps of [82]. In addition to the random error in their $E(B-V)$ values, there is a correlated uncertainty in the conversion from dust column density to extinction of 10%. This affects the nearby and distant SN differently because distant SN searches usually target regions of low galactic extinction and observe at longer wavelengths.

Gravitational lensing Gravitational lensing is expected to cause increased dispersion in the Hubble diagram of high-redshift SNe. While the mean amount of magnification is unity, when there are a small number of SN in each redshift bin, the asymmetric nature of the lensing probability, coupled with selection effects, can produce biases in the peak luminosities. For surveys over very small areas, lensing will also induce correlations between different SNe. These issues are studied in [83], who find that for current surveys, the number of SNe in each redshift range, and the survey area are large enough that these issues are minor. Lensing does induce additional, almost uncorrelated, scatter in the peak magnitudes, which can be included in the statistical error budget.

Gray dust Gray dust is a concept originally introduced to explain the faintness of the high-redshift SNe Ia when discovered in 1998, dust with negligible telltale reddening or additional dispersion. In its simplest form it can be easily tested against SN Ia observations, as it makes very different predictions for the Hubble diagram at $z > 1$. At these epochs, the SNe Ia probe the era of deceleration and will not get fainter at the same rate as that predicted by simple gray dust models [67].

A more pernicious kind of gray dust has been suggested by [84]. Theses are "replenishing dust" models, in which a constant density of gray dust is replenished at just the rate it is diluted by the expanding universe. Such models are virtually indistinguishable from that of an accelerating universe by just using the distance–redshift relation, as the dimming is directly proportional to distance traveled and mathematically similar to the effects of a cosmological constant. Dust of this sort with the required opacity, replenishing rate, and ejection velocity from galaxies ($>$1,000 km s^{-1} for it to fill space uniformly without adding detectable dispersion) is virtually undetectable in the Hubble diagram of SNe Ia. However, such dust models

involve a large amount of fine tuning and appear contrived to be a simple alternative to dark energy.

4.2 Implementation of Systematic Errors

To include these identified systematic errors in the cosmological fits, (14) can be generalized by constructing a covariance matrix $\mathbf{V}$ to replace the σ terms. $\mathbf{V}$ is the combination of a systematics covariance matrix $\mathbf{V}_{\rm syst}$ and a (diagonal) statistical covariance matrix $\mathbf{V}_{\rm stat}$ generated from the statistical errors described above. We then minimize the χ^2 according to

$$\chi^2 = \sum_N \left(\mathbf{m_B} - \mathbf{m_B^{mod}}\right)^T \mathbf{V}^{-1} \left(\mathbf{m_B} - - - \mathbf{m_B^{mod}}\right) . \tag{16}$$

This (clearly) makes the cosmological fits more computationally expensive, but allows the uncertainties on the fit parameters to directly include systematic errors, as well as correctly accounting for systematics which induce correlations between different SNe and thus alter the position of the best-fit cosmological model.

The typical magnitude of the effect on the measurement of $\langle w \rangle$ of these identified systematic effects can be found in Table 1, and Fig. 8 shows the effect on the cosmological contours [77, 74]. The typical uncertainty in $\langle w \rangle$ increases from $\sim$4.5% when only considering statistical error to $\sim$7% when including systematics. Clearly, systematic errors are a large component of the total error budget – current constraints on $\langle w \rangle$ are systematics limited. However, there are many reasons to believe that this situation will radically improve as discussed in the next section.

Table 1 Example SN Ia systematic errors on $\langle w \rangle$ for a typical SN Ia sample

Systematic	Error in $\langle w \rangle$ (stat. + this sys.)[a]	Extra error from this systematic[b]
Stat. only	4.3	...
High-z zero points	4.5	1.3
Low-z zero points	4.7	1.9
Filter responses	4.5	0.9
Photometric reference colors	5.1	2.6
SN color relation	5.0	2.5
Peculiar velocities	4.4	0.5
Malmquist bias	4.4	0.7
Non-Ia contamination	4.4	0.7
Total	7.0	5.8

[a] The total error on $\langle w \rangle$ when considering the statistical only error, plus the additional error from this systematic.
[b] The additional error in $\langle w \rangle$ from this systematic error alone.

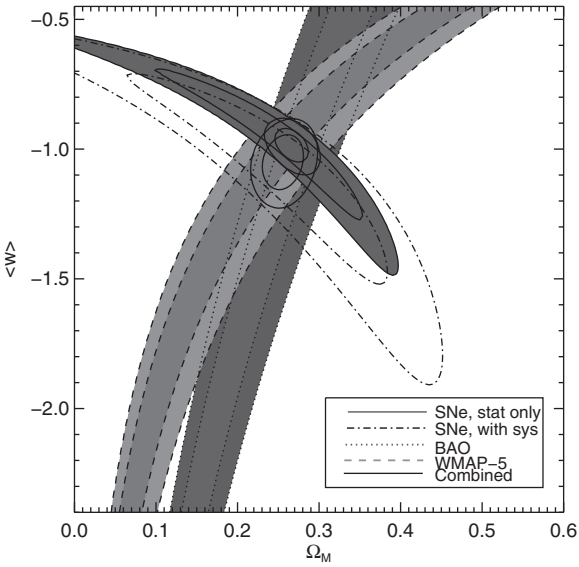

Fig. 8 As Fig. 7, but showing the effect of including SN Ia systematic errors when performing the cosmological fits. The *filled contours* are statistical only, and the *dashed contours* include the SN systematic errors

4.3 Prospects for Improvement

A careful reading of Sect. 4.1 will reveal that most of the dominant systematics are related to the current low-redshift data set and the necessity to cross-calibrate them to higher-redshift surveys such as SNLS. Since a large number of dramatically improved low-redshift data samples should become available in the next few years, observed in the same photometric system as the high-redshift data, it is worth asking exactly which aspects of these samples will help us reduce these errors.

The dominant systematics are the colors of the photometric reference standard BD 17° 4708, the differences between light-curve fitters and the zero points of the low-redshift samples. How will new low-redshift samples help with all of these? The uncertainties related to the color of BD 17° 4708 include large terms related to how well the Landolt magnitudes of this sub-dwarf can be transferred to the SNLS system. Because it is a slightly unusual star, and because the SNLS bandpasses are very unlike the Landolt ones used for measurements of the standard stars, these errors are large. Furthermore, the bandpasses of the Landolt system are simply not well understood, and never will be, putting a fundamental limit on how well this uncertainty can be characterized. Were the low-redshift sample replaced with one observed on a better understood system more similar to the SNLS or SDSS systems, these transfer effects would be minimized, substantially reducing the calibration errors. The low-redshift sample zero points can obviously be improved by better nearby samples. The effects on the SNLS/SDSS zero points are more subtle, but if these surveys are calibrated directly against a more similar system, they will be moderately reduced.

The differences between light-curve models will also be reduced with better training samples. While including high-redshift SN data in the training has been very useful, especially in the near-UV, new low-redshift samples can improve the situation even further. A particular lack in high-redshift data is multiple epochs of spectroscopy at different phases of the light curve. The uncertainty in the SN Ia color relations should also be substantially improved by new low-redshift samples simply because they dramatically increase the available pool of observations. These larger samples may allow an understanding of the various degeneracies between intrinsic and extrinsic SN Ia color by studying SNe Ia in a variety of environments, which could lead to qualitative improvements in SN Ia models.

The *Hubble Space Telescope* CALSPEC calibration used for BD 17° 4708 will also be refined and extended to more stars, particularly fainter examples that can be observed directly by modern survey telescopes, and of normal spectral types in the color range well sampled by standard star catalogs so that their magnitudes can be accurately transferred between systems. This program needs to be performed while the natural systems for high-redshift SN surveys (e.g., SDSS, SNLS) still exist; a major problem with the Landolt system is that its natural system does not – there will always be limitations as to how accurately any given flux standard can be tied to this system. This has implications for future absolute calibration programs. From the standpoint of SN observations, it is currently more important that the calibrated flux standard be tied to the magnitude system in use than how well the SED itself is calibrated, so good quality observations of fainter (and hence directly observable) standards are vastly preferable to improved observations of very bright standards such as Vega.

4.4 Further Astrophysical Systematics?

While the challenge of photometrically calibrating the physical SN Ia fluxes is considerable (Sect. 4.1), this is at least a well-defined and tractable problem on which substantial progress has been made. More concerning and pernicious is the possibility of intrinsic variability in the SN Ia population that cannot be empirically controlled. The most significant concerns are related to the unknown, or at least uncertain, astrophysical nature of the SN Ia events [e.g., 21].

Dramatic evolution in SN Ia properties is, however, ruled out. The spectra of SNe Ia are very similar across the entire redshift range in which they have been studied [e.g., 85–88], implying that the underlying physical process governing their explosions is not changing dramatically. Furthermore, SNe Ia in different type of host galaxies show very similar best-fitting cosmological models [89]. Different galaxy environments probe a large range of potential progenitor SN Ia stellar populations, from starburst galaxies with dominant young populations of stars, through normal galaxies with a substantial fraction of evolved stellar mass, to the old, evolved elliptical galaxies comprised of more homogeneous and old stellar populations. Hence their broad similarity among galaxy types is a powerful limit on the degree to which they can evolve.

However, it is well known that SNe Ia do have some connection with their host galaxy types. Although some SNe Ia occur in passive systems with no ongoing star formation, consistent with a long "delay time" from stellar birth to SN explosion, most events occur in star-forming galaxies, suggesting a shorter delay time [90, 91]. A strong correlation between the SN Ia rate and host galaxy star-formation rate is seen at all redshifts (Fig. 9). The most straightforward interpretation of this environmentally dependent SN Ia rate is a wide range of delay times, but the exact physical implications are unclear. For example, the SNLS relation between the SN Ia rate and star-formation rate implies that around 1% of all white dwarfs end their lives as SNe Ia [92], independent of their initial mass. As the single degenerate model typically has lower conversion efficiencies at lower masses, this suggests that some other mechanism is responsible for the production of at least some SNe Ia. However, the precise implication for the progenitor systems must await the construction of more detailed delay-time distributions, requiring more precise data on their host galaxies.

The "prompt" and "delayed" SNe Ia also possess different light curves. A trend of SN Ia luminosity – or equivalently stretch – versus galaxy morphological type has been observed [e.g., 93]: high-stretch SNe Ia are preferentially located in morphologically late-type galaxies (Fig. 10). This trend has also been observed when using host galaxy specific star-formation rates (sSFR; the SFR per unit stellar mass) instead of morphology [91]. The evidence suggests that prompt SNe Ia appear

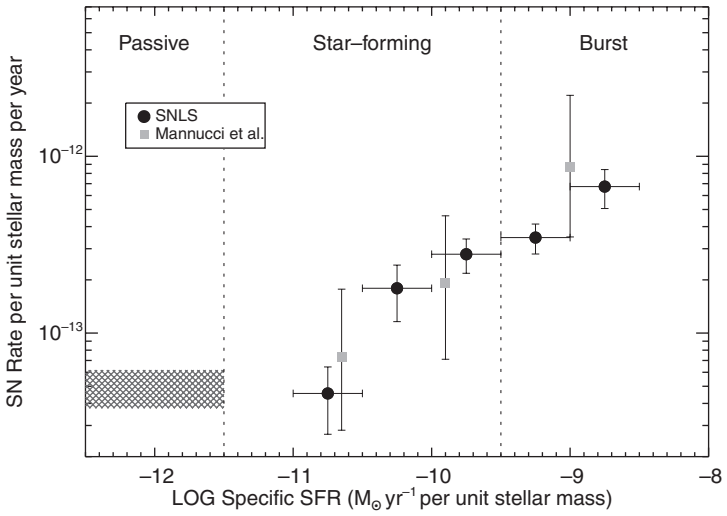

Fig. 9 The number of SNe Ia per unit stellar mass as a function of the star-formation rate (SFR) per unit stellar mass of the host galaxy. *Circles* represent SNLS data-points in star-forming galaxies. The *hashed area* shows the number per unit stellar mass as measured in the SNLS passive galaxies (assigned zero SFR). Shown for comparison (*square points*) is the evolution in SN Ia rate to later type galaxies observed locally by [90], normalized to the SNLS rate in passive galaxies. The *vertical dotted lines* show the division used to classify the host galaxies into different types. From Sullivan et al. [91], Fig. 6. Reproduced by permission of the AAS

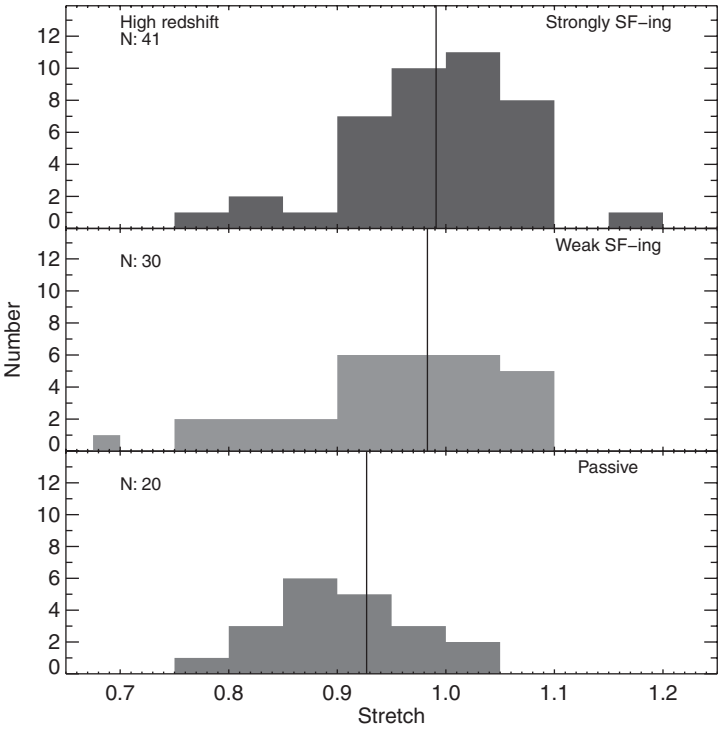

Fig. 10 The distribution of the SN Ia light-curve shape parameter "stretch" for SNLS high-redshift SNe, separated according to the specific star-formation rate of the host galaxy. The typical precision on the stretch measure is $\pm 0.01 - 0.02$, i.e., smaller than the bin width of the histograms. The *top panel* shows galaxies with a specific SFR (sSFR) of $\log(\text{sSFR}) > -9.5$, the *middle panel* galaxies with $-12.0 \leq \log(\text{sSFR}) \leq -9.5$, and the lower panel galaxies with $\log(\text{sSFR}) < -12.0$. The *vertical lines* show the positions of the median stretch in each histogram. From Sullivan et al. [91], Fig. 11. Reproduced by permission of the AAS

brighter with broader (higher stretch) light curves, while the delayed component are fainter with fast light curves – recall "stretch" is a key observable affecting the utility of SNe Ia as cosmological probes (see Sect. 3.1), correcting the luminosity of SNe Ia according to the width of their light curves. It is unclear whether the trends are primarily driven by progenitor age (passive systems hosting older stars) or progenitor metallicity (passive systems being the most massive and likely metal rich).

Regardless of the physical cause, the dependence of stretch on the apparent age of the SN Ia progenitor will lead to a subtle shift in the demographics of the SN Ia population. As the star-formation rate of the universe increases dramatically with look-back time, there will be many more prompt SNe Ia at high redshift than would be expected in the local universe. The consequence is that the high-redshift universe should have a more prevalent population of younger, higher stretch SNe than seen

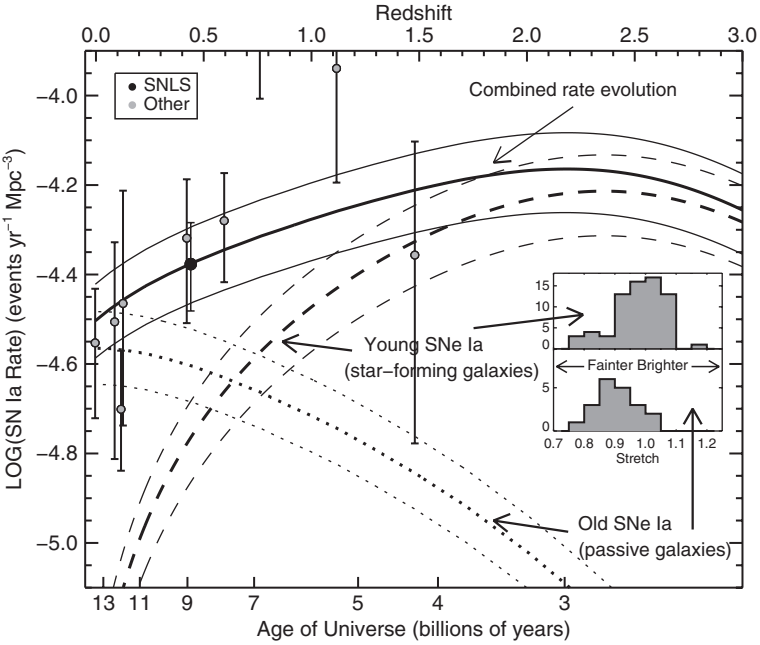

Fig. 11 The evolution of the volumetric SN Ia rate with redshift (*solid line*), based on a simple prompt (*dashed*) + delayed (*dotted*) SN Ia rate model [91]. The *inset* shows the distribution of the stretch of the SN Ia light curve associated with each of the two components — see also Fig. 10. This will lead to a subtle shift in the SN Ia stretch with redshift, as the demographics of the SN Ia population is changed

at low redshift – the mean stretch of the SN Ia population should evolve to be larger at higher redshift (Fig. 11).

Using data from various searches, this has now been tested using SN Ia data [94]. An increase in the average stretch with redshift is seen in the data, consistent with the empirical models, corresponding to $\sim$10% increase in the intrinsic SN Ia luminosity with redshift. Note that this difference is calibrated via the stretch–luminosity relationship, however, the degree to which the correction functions across the entire redshift range is still being studied.

There are also open questions as to how the metallicity or age of the progenitor star may influence the observed properties and luminosities of the SN Ia explosion, again leading to possible biases as the demographics of the SN Ia population shifts slightly with look-back time [94, 95]. Reference [96] argue dramatic changes in SN Ia physics with metallicity. They argue that synthesized ^{56}Ni mass should be linearly proportional to progenitor metallicity. Since the decay of ^{56}Ni drives the luminosity, SNe Ia in high metallicity environments should be less luminous. This is because stars from higher metallicity environments will end up with larger mass fractions of ^{22}Ne and ^{56}Fe after helium burning. Since these isotopes have excess neutrons, the authors argue that in these cases fewer radioactive elements are

produced during the process of burning to nuclear statistical equilibrium during a SN Ia. Note that these results are in sharp contrast to other studies which found no significant increase in ^{56}Ni with increasing metallicity [e.g., 97, 98]

Reassuringly, no definitive evidence for a dependence of SN Ia luminosity on inferred host galaxy metallicity has yet been uncovered [e.g., 99, 100]. Figure 12 shows the Hubble diagram residual as a function of inferred SN host galaxy metallicity for a sample of SNe Ia from the first year of the SNLS; no trend is apparent. Improved samples of SN data at both low and high redshifts should provide further constraints on the role of metallicity in influencing SN Ia luminosities.

An alternative approach is to explore the possible effects of progenitor metallicity through blanketing and wavelength-dependent features in the rest-frame UV spectra, corresponding to λλ 290–350 nm. This is a relatively unexplored region observationally as the atmosphere is opaque at these wavelengths: indeed the most complete studies have been conducted on high-redshift events where the UV spectral region is redshifted into the optical. Reference [97] argue that direct traces of the progenitor metallicity can best be seen in the unburned SN layers which are only observable significantly before maximum light. However, they also predict that an increase in progenitor metallicity will cause an increase in the amount of ^{54}Fe synthesized in the explosion, and this will result in an increase in line opacity in the UV region which may be observable at maximum light. The net effect is that an increased metallicity will result in an *increase* in the UV pseudo-

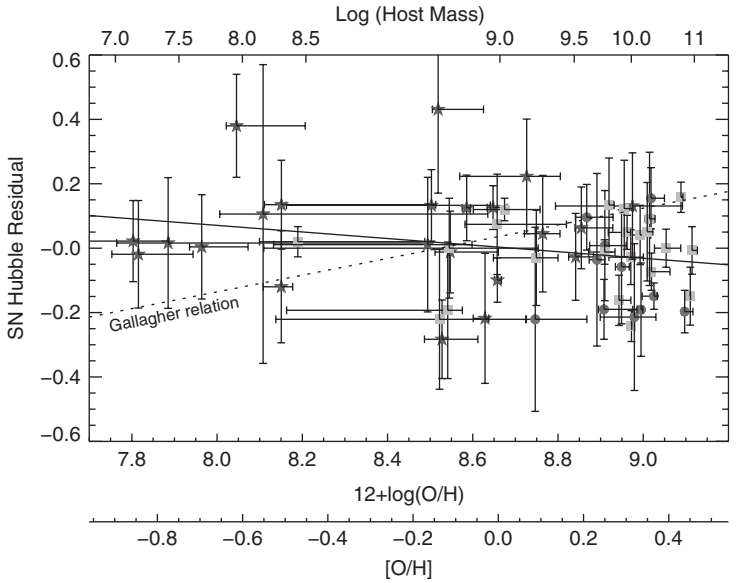

Fig. 12 Hubble residual versus inferred host galaxy metallicity for SNe Ia from the SNLS first-year sample [39]. The *solid line* is a fit to the data, consistent with zero at the 1σ level. The *dotted line* shows the relationship measured by [99], here ruled out by the data. From Howell et al. [100], Fig. 11. Reproduced by permission of the AAS

continuum at maximum light. Reference [101] examines the spectroscopic implications in greater detail. They simultaneously change the progenitor metallicity in the unburned C+O region and increase the amount of ^{54}Fe in the partially burned region. They find an increase in the level of the UV pseudo-continuum: as metallicity decreases so the line opacity decreases with the result that lines form deeper in the atmosphere and therefore from a lower velocity region. Such an effect is *opposite* to the effect predicted by [97]. However, [101] caution that the overall UV flux level is not necessarily a good indicator of metallicity, as it is dependent on many variables such as the temperature, density, and velocity of the C+O layer.

Various authors predict that the SN Ia rate should be affected by metallicity, although they do not make explicit predictions about the resulting effects on SN Ia properties. Reference [102] argues that in very low metallicity environments ($[Fe/H] < -1$) the white dwarf wind that they believe is essential for producing SNe Ia will be inhibited, thus leading to fewer SNe Ia. Reference [103] find that metallicity differences should alter the range of progenitor masses that produce SNe Ia.

In summary, therefore, theory cannot yet offer a clear consensus as to the effects of metallicity on SNe Ia. Indeed, there is disagreement not only about which effects are the most important, but also about the sign of any possible effect. This is a very challenging theoretical problem hindered by correlations between the wanted effect of metallicity and other correlations such as the viability of certain progenitor systems, the explosion mechanism and radiative transfer in an atmosphere under a variety of mixing conditions. Full simulations of all these effects may soon become feasible, but substantial campaigns will still be needed to track statistical shifts with metallicity.

Finally, there is the complex question of SN Ia colors. Their host galaxies span the full range of age from dwarf irregular galaxies through to giant ellipticals and contain vastly different amounts of dust. As discussed in Sect. 3.1, this dust has the effect of dimming the light from objects as it passes through, preferentially in the ultraviolet and blue spectral regions. But observed SN Ia properties seem inconsistent with known dust properties of the Milky Way. Probably, the question of dust represents the most serious challenge to SN Ia cosmology.

Observing SNe Ia at redder wavelengths where the effect of dust is smaller is one obvious potential solution. Observations of SNe in the rest-frame J and H bandpasses, which probe above 1 μm into the near infrared (IR), show a dramatically decreased dispersion on Hubble diagrams [e.g., 104]. SN Ia theory also suggests that any intrinsic variability in the population is smaller at these wavelengths [32]; in fact SNe Ia may be true standard candles without any need for a light-curve shape correction [24]. The problem with this approach is that near-IR observations are very challenging from the ground due to the increased sky brightness: to date observations are limited to a redshift of about 0.5. Space-based missions will be required to push this further for large samples of SNe.

While these potential systematics may appear serious, in part, this is because the SN Ia technique is the most mature and tested probe of dark energy. Despite many

decades of intensive searching, no fatal flaw has yet been identified – and SNe Ia have, so far, passed many detailed examinations of systematic effects with flying colors.

5 Concluding Remarks

Current SN Ia data sets play an integral part in making the most precise measurements of the dark energy driving the accelerating universe. At the same time, modern SN surveys also allow new insights into the astrophysics governing SN Ia progenitors. No effect has yet been uncovered that challenges the conclusions drawn from the use of SNe Ia in cosmological applications, but some open questions do remain. Why are the brightest SNe Ia associated with short delay times and young galaxies? How well do SNe Ia from different environments inter-calibrate in a cosmological analysis? A tantalizing possibility is the existence of *more than one progenitor mechanism*. The key to making progress is to pinpoint any fundamental environmental differences between the delayed and prompt events; several programs are underway to probe these questions.

In this regard, SN Ia observations seem in a particularly healthy state given the large number of proposed SN Ia surveys (Table 2). At low redshift, at least three new rolling SN Ia surveys are either planned or have commenced operation – the Palomar Transient Factory, the SkyMapper, and the La Silla SN Search. These surveys will generate many thousands of new SN Ia events, and ultimately studying these objects in details will lead to new insights into their progenitor systems and physics. At higher redshift, the Dark Energy Survey will eventually supplant the existing SNLS data set over the course of the next 5–7 years. The prospects for an eventual space-based mission to study dark energy are good, and SNe Ia are likely to be studied in detail by such an experiment.

As with any experimental technique, the final precision of the SN Ia cosmological results is governed by both statistical and systematic uncertainties. As discussed in this chapter, as more SNe Ia are used in the analysis and the statistical error decreases, the contribution of systematic errors has become increasingly important. Ultimately, the challenge of controlling systematics in SN cosmology is twofold.

Table 2 A selection of upcoming and planned SN Ia experiments

Time	$z < 0.1$	$0.1 < z < 1.0$	$z > 1$
Now	KAIT/CfA/CSP ∼300 SNFactory ∼100	SNLS ∼450 Essence ∼200 SDSS ∼ 250	HST/GOODS ∼20 HST/Clusters ∼20
2009–2013	SkyMapper PTF La Silla	DES PANSTARRS	HST/WFC3
2013++		LSST $\sim n \times 10^4$ JDEM	JDEM JWST TMT/ELTs

The first is photometric calibration; future, planned experiments will require a calibration of better than 1% in both the distant and nearby samples. The second is understanding the limitations of SNe Ia by investigating their astrophysical properties and, ultimately, controlling any subtle evolutionary effects that may emerge. This is the challenge for the next few years of SN Ia observation and theory.

Acknowledgments I acknowledge support from the Royal Society.

References

1. E. Hubble, Proc. Natl. Acad. Sci. **15**, 168 (1929). DOI 10.1073/pnas.15.3.168
2. E. Hubble and M.L. Humason, Astrophys. J. **74**, 43 (1931). DOI 10.1086/143323
3. P.J. Peebles and B. Ratra, Rev. Modern Phy. **75**, 559 (2003)
4. E.J. Copeland, M. Sami and S. Tsujikawa, Int. J. Modern Phys. D **15**, 1753 (2006). DOI 10.1142/S021827180600942X
5. A. Lue, R. Scoccimarro and G. Starkman, Phys. Rev. D **69**(4), 044005 (2004). DOI 10.1103/PhysRevD.69.044005
6. J. Peacock and P. Schneider, The Messenger **125**, 48 (2006)
7. A. Albrecht, G. Bernstein, R. Cahn, W.L. Freedman, J. Hewitt, W. Hu, J. Huth, M. Kamionkowski, E.W. Kolb, L. Knox, J.C. Mather, S. Staggs and N.B. Suntzeff, ArXiv Astrophysics e-prints (2006)
8. R. Trotta and R. Bower, Astron. Geophys. **47**(4), 040000 (2006). DOI 10.1111/j.1468-4004.2006.47420.x
9. J.A. Frieman, M.S. Turner and D. Huterer, Annu. Rev. Astron. Astrophys. **46**, 385 (2008). DOI 10.1146/annurev.astro.46.060407.145243
10. S.M. Carroll, W.H. Press and E.L. Turner, Annu. Rev. Astron. Astrophys. **30**, 499 (1992)
11. G. Efstathiou, W.J. Sutherland and S.J. Maddox, Nature **348**, 705 (1990). DOI 10.1038/348705a0
12. L.M. Krauss and M.S. Turner, Gen. Rel. Grav. **27**, 1137 (1995). DOI 10.1007/BF02108229
13. J.P. Ostriker and P.J. Steinhardt, Nature **377**, 600 (1995). DOI 10.1038/377600a0
14. W.L. Freedman, et al., Astrophys. J. **553**, 47 (2001). DOI 10.1086/320638
15. E.V. Linder, Phys. Rev. Lett. **90**(9), 091301 (2003). DOI 10.1103/PhysRevLett.90.091301
16. P.S. Corasaniti and E.J. Copeland, Phys. Rev. D **67**(6), 063521 (2003). DOI 10.1103/PhysRevD.67.063521
17. D. Huterer and G. Starkman, Phys. Rev. Lett. **90**(3), 031301 (2003). DOI 10.1103/PhysRevLett.90.031301
18. V. Sahni and A. Starobinsky, Int. J. Modern Phys. D **15**, 2105 (2006). DOI 10.1142/S0218271806009704
19. R.A. Daly, S.G. Djorgovski, K.A. Freeman, M.P. Mory, C.P. O'Dea, P. Kharb and S. Baum, Astrophys. J. **677**, 1 (2008). DOI 10.1086/528837
20. A.M. Khokhlov, Astron. Astrophys. **245**, 114 (1991)
21. W. Hillebrandt and J.C. Niemeyer, Annu. Rev. Astron. Astrophys. **38**, 191 (2000). DOI 10.1146/annurev.astro.38.1.191
22. S.A. Colgate and C. McKee, Astrophys. J. **157**, 623 (1969). DOI 10.1086/150102
23. M.J. Kuchner, R.P. Kirshner, P.A. Pinto and B. Leibundgut, Astrophys. J. **426**, L89+ (1994). DOI 10.1086/187347
24. D. Kasen, F. Roepke and S.E. Woosley, ArXiv e-prints (2009)
25. C.T. Kowal, Astron. J. **73**, 1021 (1968)
26. H.U. Norgaard-Nielsen, L. Hansen, H.E. Jorgensen, A. Aragon Salamanca and R.S. Ellis, Nature **339**, 523 (1989). DOI 10.1038/339523a0

27. S. Perlmutter, et al., Astrophys. J. **483**, 565 (1997). DOI 10.1086/304265
28. B.P. Schmidt, et al., Astrophys. J. **507**, 46 (1998). DOI 10.1086/306308
29. A.G. Riess, et al., AJ **116**, 1009 (1998). DOI 10.1086/300499
30. S. Perlmutter, et al., The Supernova Cosmology Project, Astrophys. J. **517**, 565 (1999). DOI 10.1086/307221
31. M.M. Phillips, Astrophys. J. **413**, L105 (1993). DOI 10.1086/186970
32. D. Kasen and S.E. Woosley, Astrophys. J. **656**, 661 (2007). DOI 10.1086/510375
33. P. Hoeflich, A. Khokhlov, J.C. Wheeler, M.M. Phillips, N.B. Suntzeff and M. Hamuy, Astrophys. J. **472**, L81+ (1996). DOI 10.1086/310363
34. P.A. Pinto and R.G. Eastman, Astrophys. J. **530**, 744 (2000). DOI 10.1086/308376
35. P.A. Pinto and R.G. Eastman, Astrophys. J. **530**, 757 (2000). DOI 10.1086/308380
36. P.A. Mazzali, K. Nomoto, E. Cappellaro, T. Nakamura, H. Umeda and K. Iwamoto, Astrophys. J. **547**, 988 (2001). DOI 10.1086/318428
37. R. Tripp, Astron. Astrophys. **331**, 815 (1998)
38. M.S. Bessell, PASP **102**, 1181 (1990). DOI 10.1086/132749
39. P. Astier, et al., Astron. Astrophys. **447**, 31 (2006). DOI 10.1051/0004-6361:20054185
40. A. Conley, R.G. Carlberg, J. Guy, D.A. Howell, S. Jha, A.G. Riess and M. Sullivan, Astrophys. J. **664**, L13 (2007). DOI 10.1086/520625
41. S. Nobili and A. Goobar, Astron. Astrophys. **487**, 19 (2008). DOI 10.1051/0004-6361:20079292
42. L. Østman, A. Goobar and E. Mörtsell, Astron. Astrophys. **485**, 403 (2008). DOI 10.1051/0004-6361:20079187
43. A. Goobar, Astrophys. J. **686**, L103 (2008). DOI 10.1086/593060
44. S. Jha, A.G. Riess and R.P. Kirshner, Astrophys. J. **659**, 122 (2007). DOI 10.1086/512054
45. J. Guy, et al., Astron. Astrophys. **466**, 11 (2007). DOI 10.1051/0004-6361:20066930
46. A. Conley, et al., Astrophys. J. **681**, 482 (2008). DOI 10.1086/588518
47. A.G. Riess, W.H. Press and R.P. Kirshner, Astrophys. J. **473**, 88 (1996). DOI 10.1086/178129
48. G. Goldhaber, et al., Astrophys. J. **558**, 359 (2001). DOI 10.1086/322460
49. R.A. Knop, et al., Astrophys. J. **598**, 102 (2003)
50. M. Hamuy, M.M. Phillips, N.B. Suntzeff, R.A. Schommer, J. Maza, R.C. Smith, P. Lira and R. Aviles, Astron. J. **112**, 2438 (1996). DOI 10.1086/118193
51. J.L. Prieto, A. Rest and N.B. Suntzeff, Astrophys. J. **647**, 501 (2006). DOI 10.1086/504307
52. J.L. Tonry, et al., Astrophys. J. **594**, 1 (2003)
53. L. Wang, G. Goldhaber, G. Aldering and S. Perlmutter, Astrophys. J. **590**, 944 (2003). DOI 10.1086/375020
54. W.M. Wood-Vasey, et al., Astrophys. J. **666**, 694 (2007). DOI 10.1086/518642
55. A.U. Landolt, Astron. J. **104**, 340 (1992). DOI 10.1086/116242
56. P. Nugent, A. Kim and S. Perlmutter, Publ. Astron. Soc. Pacific **114**, 803 (2002). DOI 10.1086/341707
57. E.Y. Hsiao, A. Conley, D.A. Howell, M. Sullivan, C.J. Pritchet, R.G. Carlberg, P.E. Nugent and M.M. Phillips, Astrophys. J. **663**, 1187 (2007). DOI 10.1086/518232
58. M. Goliath, R. Amanullah, P. Astier, A. Goobar and R. Pain, Astron. Astrophys. **380**, 6 (2001). DOI 10.1051/0004-6361:20011398
59. A.A. Penzias and R.W. Wilson, Astrophys. J. **142**, 419 (1965). DOI 10.1086/148307
60. M.R. Nolta, et al., Astrophys. J. **180**, 296 (2009). DOI 10.1088/0067-0049/180/2/296
61. J. Dunkley, et al., Astrophys. J. **180**, 306 (2009). DOI 10.1088/0067-0049/180/2/306
62. P.J.E. Peebles and J.T. Yu, Astrophys. J. **162**, 815 (1970). DOI 10.1086/150713
63. J.R. Bond and G. Efstathiou, MNRAS **226**, 655 (1987)
64. C. Blake and K. Glazebrook, Astrophys. J. **594**, 665 (2003). DOI 10.1086/376983
65. H.J. Seo and D.J. Eisenstein, Astrophys. J. **598**, 720 (2003). DOI 10.1086/379122
66. H.J. Seo and D.J. Eisenstein, Astrophys. J. **665**, 14 (2007). DOI 10.1086/519549
67. A.G. Riess, et al., Astrophys. J. **607**, 665 (2004)
68. A.G. Riess,et al., Astrophys. J. **659**, 98 (2007). DOI 10.1086/510378

69. M. Hamuy, et al., AJ **112**, 2408 (1996). DOI 10.1086/118192
70. S. Jha, et al., AJ **131**, 527 (2006). DOI 10.1086/497989
71. M. Hamuy, et al., PASP **118**, 2 (2006). DOI 10.1086/500228
72. M. Hicken, et al., Astrophys. J. **700**, 331 (2009). DOI 10.1088/0004-637X/700/1/331
73. A. Rau, et al., ArXiv e-prints (2009)
74. M. Sullivan, et al., in *Astrophys. J.,* submitted (2010)
75. D.J. Eisenstein, et al., Astrophys. J. **633**, 560 (2005). DOI 10.1086/466512
76. E. Komatsu, et al., Astrophys. J. **180**, 330 (2009). DOI 10.1088/0067-0049/180/2/330
77. A.J. Conley, et al., Astrophys. J., submitted (2010)
78. N. Regnault, et al., Astron. Astrophys. **506**, 999 (2009)
79. N.L. Homeier, Astrophys. J. **620**, 12 (2005). DOI 10.1086/427060
80. L. Hui and P.B. Greene, Phys. Rev. D **73**(12), 123526 (2006). DOI 10.1103/PhysRevD.73.123526
81. J.D. Neill, M.J. Hudson and A. Conley, Astrophys. J. **661**, L123 (2007). DOI 10.1086/518808
82. D.J. Schlegel, D.P. Finkbeiner and M. Davis, Astrophys. J. **500**, 525 (1998). DOI 10.1086/305772
83. D.E. Holz and E.V. Linder, Astrophys. J. **631**, 678 (2005). DOI 10.1086/432085
84. A. Goobar, L. Bergström and E. Mörtsell, Astron. Astrophys. **384**, 1 (2002). DOI 10.1051/0004-6361:20020002
85. I.M. Hook, et al., Astron. J. **130**, 2788 (2005). DOI 10.1086/497635
86. S. Blondin, et al., Astron. J. **131**, 1648 (2006). DOI 10.1086/498724
87. R.S. Ellis, et al., Astrophys. J. **674**, 51 (2008). DOI 10.1086/524981
88. M. Sullivan, R.S. Ellis, D.A. Howell, A. Riess, P.E. Nugent and A. Gal-Yam, Astrophys. J. **693**, L76 (2009). DOI 10.1088/0004-637X/693/2/L76
89. M. Sullivan, et al., MNRAS **340**, 1057 (2003)
90. F. Mannucci, M. della Valle, N. Panagia, E. Cappellaro, G. Cresci, R. Maiolino, A. Petrosian and M. Turatto, Astron. Astrophys. **433**, 807 (2005). DOI 10.1051/0004-6361:20041411
91. M. Sullivan, et al., Astrophys. J. **648**, 868 (2006). DOI 10.1086/506137
92. C.J. Pritchet, D.A. Howell and M. Sullivan, Astrophys. J. **683**, L25 (2008). DOI 10.1086/591314
93. M. Hamuy, S.C. Trager, P.A. Pinto, M.M. Phillips, R.A. Schommer, V. Ivanov and N.B. Suntzeff, Astron. J. **120**, 1479 (2000). DOI 10.1086/301527
94. D.A. Howell, M. Sullivan, A. Conley and R. Carlberg, Astrophys. J. **667**, L37 (2007). DOI 10.1086/522030
95. D. Sarkar, A. Amblard, A. Cooray and D.E. Holz, Astrophys. J. **684**, L13 (2008). DOI 10.1086/592019
96. F.X. Timmes, E.F. Brown and J.W. Truran, Astrophys. J. **590**, L83 (2003). DOI 10.1086/376721
97. P. Höflich, J.C. Wheeler and F.K. Thielemann, Astrophys. J. **495**, 617 (1998)
98. K. Iwamoto, F. Brachwitz, K. Nomoto, N. Kishimoto, H. Umeda, W.R. Hix and F.K. Thielemann, Astrophys. J. **125**, 439 (1999). DOI 10.1086/313278
99. J.S. Gallagher, P.M. Garnavich, N. Caldwell, R.P. Kirshner, S.W. Jha, W. Li, M. Ganeshalingam and A.V. Filippenko, Astrophys. J. **685**, 752 (2008). DOI 10.1086/590659
100. D.A. Howell, et al., Astrophys. J. **691**, 661 (2009). DOI 10.1088/0004-637X/691/1/661
101. E.J. Lentz, E. Baron, D. Branch, P.H. Hauschildt and P.E. Nugent, Astrophys. J. **530**, 966 (2000)
102. C. Kobayashi, T. Tsujimoto, K. Nomoto, I. Hachisu and M. Kato, Astrophys. J. **503**, L155+ (1998). DOI 10.1086/311556
103. N. Langer, A. Deutschmann, S. Wellstein and P. Höflich, Astron. Astrophys. **362**, 1046 (2000)
104. W.M. Wood-Vasey, et al., Astrophys. J. **689**, 377 (2008). DOI 10.1086/592374

http://www.springer.com/978-3-642-10597-5

Lectures on Cosmology
Accelerated Expansion of the Universe
Wolschin, G. (Ed.)
2010, X, 200 p. 30 illus., Softcover
ISBN: 978-3-642-10597-5